JOURNAL OF GEOPHYSICAL RESEARCH, VOL. 100, NO. D8, PAGES 16,699–16,720, AUGUST 20, 1995

# Seasonal evolutions of $N_2O$, $O_3$, and $CO_2$: Three-dimensional simulations of stratospheric correlations

Timothy M. Hall [1]

NASA Goddard Institute for Space Studies and Columbia University, New York

Michael J. Prather

Earth System Science Department, University of California, Irvine

**Abstract.** Fluctuations in the concentrations of stratospheric trace gases are often correlated over a large range of space and time scales, an observation frequently used to infer the existence of various chemical processes. Three-dimensional models provide a tool to examine the causes and variations of trace gas relationships, because they can realistically simulate the interplay between stratospheric photochemistry and meteorology. Thus such models can aid the interpretation of observed trace gas relationships. We use the general circulation model of the Goddard Institute for Space Studies to simulate the evolution and distribution of $N_2O$, $CO_2$, and $O_3$ over a year. In the modeled lower stratosphere the constituents $N_2O$ and $CO_2$ have well-correlated spatial variations, but the slope of the regression line depends on both the season and the direction of sampling. This departure from a universal form is due both to the annual cycle in tropospheric $CO_2$ and to transport of air from the upper stratosphere photochemically depleted in $N_2O$. Due to the short photochemical lifetime of tropical $O_3$, its relationship with $N_2O$ is still more varied. In particular, the slope of the $O_3$–$N_2O$ regression line changes significantly from middle to high latitudes, behavior relevant to the use of $N_2O$ for estimating the rate of polar winter $O_3$ depletion. In general, a tight correlation between two trace gases such as $N_2O$ and $O_3$ is often observed, but this datum cannot be used to infer a similar universal relationship because a different direction of sampling may change the slope and the scatter about it.

## 1. Introduction

Trace gases in the stratosphere are observed to vary rapidly in space and time. Only photochemical reactions can create or destroy a given species. Dynamical motions are responsible for the mixing of air parcels with different chemical histories. Thus observed variations in trace gases involve an interplay between chemical creation of gradients and dynamical relaxation of these structures. A major challenge to the interpretation of measurements and to their comparison with models is to separate and evaluate the roles of each process.

Observations of mixing ratios for the long-lived trace gases, such as $CH_4$ and $N_2O$, show on average large-scale features that are functions of latitude and altitude. When these climatic patterns are removed, there remains substantial variability from observation to observation. *Ehhalt et al.* [1983] showed that a large fraction of these residual variations are correlated across a variety of species, including $O_3$ in the lower stratosphere. They interpret the observed variability as meteorology acting on the climatic patterns. *Mahlman et al.* [1986] used a three-dimensional model of the general circulation to show that these tracer correlations would be expected for species with local chemical lifetimes longer than a year. Recent in situ measurements from several aircraft campaigns have greatly expanded these correlative data sets, with greater precision and more species, but are limited to below 20 km altitude (the campaigns and their introductory references are the Airborne Antarctic Ozone Experiment (AAOE) [*Tuck et al.*, 1989], the Airborne Antarctic Stratospheric Experiment (AASE) [*Turco et al.*, 1990], the Stratosphere-Troposphere Exchange Project (STEP) [*Pfister et al.*, 1991], STEP/Tropical [*Pfister and Russell*, 1993], and AASE-II [*Anderson and Toon*, 1993]). In addition to motivating a theory for the regression slope of one tracer

[1] Now at CRC for Southern Hemisphere Meteorology, Monash University, Notting Hill, Australia.



Paper number 94JD03300.
0148-0227/95/94JD-03300$05.00

against another [*Plumb and Ko*, 1992], many of these measurements have been used to infer chemical processing in the stratosphere, such as denitrification over the winter poles [*Fahey et al.*, 1990] and ozone loss in the lower stratosphere [*Strahan et al.*, 1989; *Schoeberl et al.*, 1990; *Proffitt et al.*, 1990; *Collins et al.*, 1993]. While clearly able to identify key processes, are these explanations unique, and how quantitative can they be made?

We believe the above interpretations require a theoretical framework in which the proposed chemical processes can interact with stratospheric meteorology, thus predicting a priori the tracer relationships. If a model is to simulate tracer variations comparable to those observed it must include realistic, day-to-day changes in the circulation of the stratosphere. We use the stratospheric version of the Goddard Institute for Space Studies (GISS) general circulation model (GCM) to simulate the distribution of $N_2O$, $CO_2$, and $O_3$ in the stratosphere, and to examine the consequent tracer relationships. Within this framework we test a range of hypothetical models to determine which properties of the chemistry control the tracer-tracer slopes observed in the lower stratosphere. Various sampling strategies (i.e., ways to make measurements) in the model stratosphere can produce compact, smoothly varying curves describing the $N_2O$–$CO_2$ relationship. However, these curves are not universal: the $N_2O$–$CO_2$ slope varies significantly with season, location, and direction of sampling. These changes can be understood in terms of separate processes involving seasonal forcing, monotonic growth, and chemical loss in the upper stratosphere. The $N_2O$–$O_3$ relationships are much less compact due to the shorter chemical timescales for $O_3$ in the lower stratosphere but clearly show a change in slope from mid to high latitudes, even without enhanced polar $O_3$ loss in the model.

The chemical transport model (CTM), including the photochemical schemes, and the meteorology provided by the GISS GCM, is documented briefly in section 2. In section 3 we show that typical observed climatic features for $N_2O$ and $O_3$ are reproduced. In particular, the model does a good job of simulating the $O_3$ gradient across the tropopause. In section 4, after presenting plots of simulated $CO_2$ versus $N_2O$ we analyze a set of hypothetical tracers that explain key features of the $N_2O$–$CO_2$ relationship. We then examine the spatial dependence of the modeled $N_2O$–$O_3$ relationship in section 5, which, if realistic, may alter some estimates of Arctic $O_3$ loss. In each section discussing tracer correlations, we begin to compare the modeled tracer relationships with observations, using a few selected, published examples. Possible directions for model development and analysis of recent observations are discussed in the concluding section 6.

## 2. The Chemical Transport Model

The CTM uses winds computed by the stratospheric GISS GCM [*Rind et al.*, 1990] to advect chemical constituents. The horizontal resolution is 7.83° latitude by 10° longitude. In the vertical, nine sigma layers represent the surface to 100 mbar, while 12 stratospheric layers (three per decade in pressure) lie between fixed pressure levels reaching to approximately 0.05 mbar. The top three layers of the 23-layer GCM are combined into the top layer of the CTM. A single year of GCM winds beginning April 1 has been stored and is recycled for multiyear CTM simulations. Thus we do not simulate the effects of interannual variations in stratospheric circulation. Parameterized convection and associated horizontal diffusion occurs in the troposphere, but not the stratosphere.

We apply boundary conditions for trace gas mixing ratios in the lowest three layers (up to 1 km altitude), as either fixed or time varying. For species with active chemistry the CTM computes production minus loss above 200 mbar using tables of zonal-mean, monthly parameters. These parameters are calculated from a detailed photochemical model [*Logan et al.*, 1978; *Remsberg and Prather*, 1993] using observed climatic values for temperature, ozone, and other trace gases [*Prather et al.*, 1990b].

The advecting algorithm conserves first- and second-order moments of the trace gas distribution in three dimensions within a grid box [*Prather*, 1986]. This scheme, although requiring the storage of nine moments in addition to the total tracer mass, nearly eliminates numerical diffusion. The additional information represented by the moments allows us to diagnose trace gas concentrations on a subgrid scale: (1) in the vertical direction a box is divided into three equal air mass layers; (2) the tracer is averaged over each sublayer (with vertical coordinates 0–1/3, 1/3–2/3, and 2/3–1); and (3) the computed mean mixing ratios by mass $f(z)$ are taken as midpoint values for each sublayer. These are

$$f(\frac{1}{6}) = \frac{1}{M_0}(S_0 - \frac{2}{3}S_Z + \frac{2}{9}S_{ZZ}) \quad (1)$$

$$f(\frac{1}{2}) = \frac{1}{M_0}(S_0 - \frac{4}{9}S_{ZZ}) \quad (2)$$

$$f(\frac{5}{6}) = \frac{1}{M_0}(S_0 + \frac{2}{3}S_Z + \frac{2}{9}S_{ZZ}) \quad (3)$$

where $M_0$ is the air mass (kilograms) of the whole grid box, and $S_0$, $S_Z$, and $S_{ZZ}$ are the total mass and first- and second-order vertical moments of the trace gas distribution, repectively, all in the same units (kilograms). This procedure is preferred to direct sampling of the quadratic polynomial describing the mixing ratio because such fits (i.e., Legendre polynomials) are poorly behaved near the edges. Using this algorithm, we linearly interpolate between subgrid values to diagnose vertical profiles on a standard grid (every 2 km in pressure altitude).

The tropospheric version of the CTM has been documented [*Prather*, 1986; *Prather et al.*, 1987]. The stratospheric CTM has been used to study meteoric in-

fall [*Prather and Rodriguez*, 1988], dilution of the ozone hole [*Prather et al.*, 1990a], the space shuttle [*Prather et al.*, 1990b], and $CO_2$ [*Hall and Prather*, 1993]. In this modeling study, the three trace gases $N_2O$, $CO_2$, and $O_3$ have no interactions. We are thus free to simulate each separately, and consider interrelationships afterwards. Details of the $CO_2$, $N_2O$, and $O_3$ simulations are described below.

### Carbon Dioxide

Emission and uptake of atmospheric $CO_2$ are not in balance today. Atmospheric concentrations have been increasing throughout the industrial era at a rate of about 1.5 ppm/yr in the 1980s [*Keeling et al.*, 1989], but much more slowly (0.5 ppm/yr) during the apparently anomalous years 1991-1993 [*Conway et al.*, 1994]. On top of this trend, there are large seasonal variations driven by the annual cycle of biospheric uptake and release of carbon. This cycle, having typical peak-to-peak amplitude at the surface as large as 14 ppm, is neither sinusoidal nor symmetric between hemispheres, but repeats regularly with some interannual variability [*Keeling et al.*, 1989]. We model $CO_2$ without chemistry in the stratosphere, and therefore neglect the small source (up to 1.5 ppm) due to $CH_4$ oxidation. The $CO_2$ simulation employed here is identical to that of *Hall and Prather* [1993]. Briefly, a time-dependent surface boundary condition on the mixing ratio has two components: (1) a steady 1.5 ppm/yr increase, and (2) a latitude-dependent, but zonally averaged, annual cycle based on obvservations. In this case the model itself, through advection by winds and monthly mean patterns of cumulus convection, determines the amplitude and phase of the $CO_2$ cycle in the troposphere. Although clearly not adequate for accurate modeling of $CO_2$ throughout the troposphere (see, e.g., *Fung et al.* [1987]), the scheme used here is sufficient for our goal of simulating the the $CO_2$ distribution in the upper troposphere and stratosphere. The influence of the steady trend reach 40 km in about 3.5 years. The annual cycle propagates into the stratosphere with a phase delay extending outward from the tropical tropopause. In the lower stratosphere this cycle has an amplitude of about 2.0 ppm peak-to-peak in the tropics attenuating to 1.0 ppm at high latitudes, with the two hemispheres in phase.

### Nitrous Oxide

A major source of $N_2O$ involves microbial activity in the soils and oceans but is clearly influenced by human activity [*Houghton et al.*, 1992]. $N_2O$ loss occurs via stratospheric dissociation and reaction with $O(^1D)$. Although atmospheric concentrations are observed to be increasing about 0.25% per year and the interhemispheric gradient is about 1 ppb, we adopted a fixed boundary condition of 300 ppb. (For the current best value of 310 ppb, the results presented here could be scaled linearly.) A table of loss frequencies is calculated with the off-line photochemical model and used to derive $N_2O$ losses at each CTM time step as a function of latitude, altitude, and month. Local loss frequencies vary from $(10\ \text{yr})^{-1}$ at 29 km to $(1\ \text{yr})^{-1}$ and greater above 37 km. We derive a global-mean lifetime (defined as total burden divided by loss) for $N_2O$ of 131 years.

Because of the exponential fall-off in $N_2O$ loss frequency with increasing pressure, the variation in $N_2O$ losses from the top to the bottom of a 5-km-thick level can be large. Thus we take advantage of the additional information in the vertical moments of the $N_2O$ distribution to calculate the losses (i.e., change in $S_0$) and redistributions of the moments (i.e., changes in $S_Z$ and $S_{ZZ}$). There is a unique solution for coupling the moment distribution of $N_2O$ with that of the loss frequency ($L_0$, $L_Z$, and $L_{ZZ}$ in $\text{s}^{-1}$):

$$\Delta S_0 = \Delta t(S_0 L_0 + \frac{1}{3} S_Z L_Z + \frac{1}{5} S_{ZZ} L_{ZZ}) \quad (4)$$

$$\Delta S_Z = \Delta t(S_0 L_Z + S_Z L_0 + \frac{2}{5} S_{ZZ} L_Z + \frac{2}{5} S_Z L_{ZZ}) \quad (5)$$

$$\Delta S_{ZZ} = \Delta t(S_0 L_{ZZ} + S_{ZZ} L_0 + \frac{2}{3} S_Z L_Z + \frac{2}{7} S_{ZZ} L_{ZZ}) \quad (6)$$

where $\Delta$ is the change in appropriate moment corresponding to a time step $\Delta t$. This new approach to utilizing the second-order moments for more than just advection (M. M. García, private communications, 1991) is exact to second order and represents a first step toward a complete coupling of the moments and the chemistry.

### Ozone

At each time step the CTM calculates a tendency for $O_3$ (e.g., ppb/d) as a function of latitude, altitude, month, and local instantaneous $O_3$ concentration. The change is applied over the time step duration $\Delta t$, typically 4 hours. We do not consider temperature variations or changes in the overhead $O_3$ column other than those represented by the monthly, zonal-mean climatic patterns. These tendancy calculations employ two parameters describing the linearization of net $O_3$ production about the climatic mean value for each location. The parameters, stored in a three-dimensional table (latitude, longitude, month) for use by the CTM, have been computed by the photochemical model using observed climatic patterns of $O_3$ and temperature, along with estimated distributions of trace gases ($CH_4$, $H_2O$, CO, $NO_y$, $Cl_y$, and $Br_y$) necessary for the photochemistry. This scheme is the same as the original "Z chemistry" $O_3$ simulation of *Prather et al.* [1990a], using "JPL-87" kinetics [*DeMore et al.*, 1987] and includes no heterogeneous processes. Above 30 km, the $O_3$ concentrations are relaxed rapidly to the observed values, rather than to the steady state from the photochemical

model. In the lower stratosphere, $O_3$ is almost never in photochemical steady state, chemical rates for $O_3$ change are slow, and the distribution is determined by a coupling of chemistry and dynamics. Thus this region provides a good test of the $O_3$ simulation. In the troposphere, below the 200 mbar level, there is no modeled photochemistry; a uniform lower boundary condition of 20 ppb is adopted for the first three layers.

## 3. Observed and Modeled Mean Distributions

### Carbon Dioxide

Published profiles for stratospheric $CO_2$ [*Schmidt and Khedim*, 1991] show a mean lag of about 4.5 years between 32 km and the troposphere. This model produces similar values [*Hall and Prather*, 1993]. The sparseness and lack of precision of these balloon soundings precludes a critical test of the propagation of the annual cycle into the lower stratosphere. New observations from aircraft (G. W. Sachse, private communications, 1994; *Boering et al.* [1994]) show evidence, although still incomplete, of this annual cycle in the lower stratosphere. For example, the October-May differences observed at 19 km in northern midlatitudes are consistent with the model. Sparseness once again limits the determination of phase and amplitude throughout the lower stratosphere, but the additional information from the correlations of $CO_2$ with $N_2O$ [*Boering et al.*, 1994] provides a more stringent model test, as discussed later.

### Nitrous Oxide

This is the first presentation of $N_2O$ modeling for the CTM. In Figure 1 the zonal-mean mixing ratio contours for January, April, July, and October display the basic observed climatic distributions from satellite data (Nimbus 7 Stratospheric and Mesospheric Sounder (SAMS)) [*Jones and Pyle*, 1984], with upwelling of $N_2O$ rich air in the tropics and descent of $N_2O$ poor air at high latitudes. We adopt the model-measurement test described by *Remsberg and Grose* [1993] to analyze the seasonal patterns of $N_2O$, recognizing the problems with SAMS $N_2O$ observations at low altitudes. Figure 2 displays the time series of the latitudinal gradient of zonal-mean $N_2O$ at 44 km for SAMS and the CTM. (Note that the vertical coordinate used for presenting model results is pressure altitude, given by $z^* = 16\log(1000/p)$, where $p$ is in millibar and $z^*$ in kilometers.) The model shows the peak upward transport of $N_2O$ shifting to follow the Sun and reproduces the discontinuity of the peak across the equator at equinox. The modeled amplitudes are in excellent agreement with SAMS, with peak values of about 30 ppb, and midlatitude values of 10 ppb. However, the

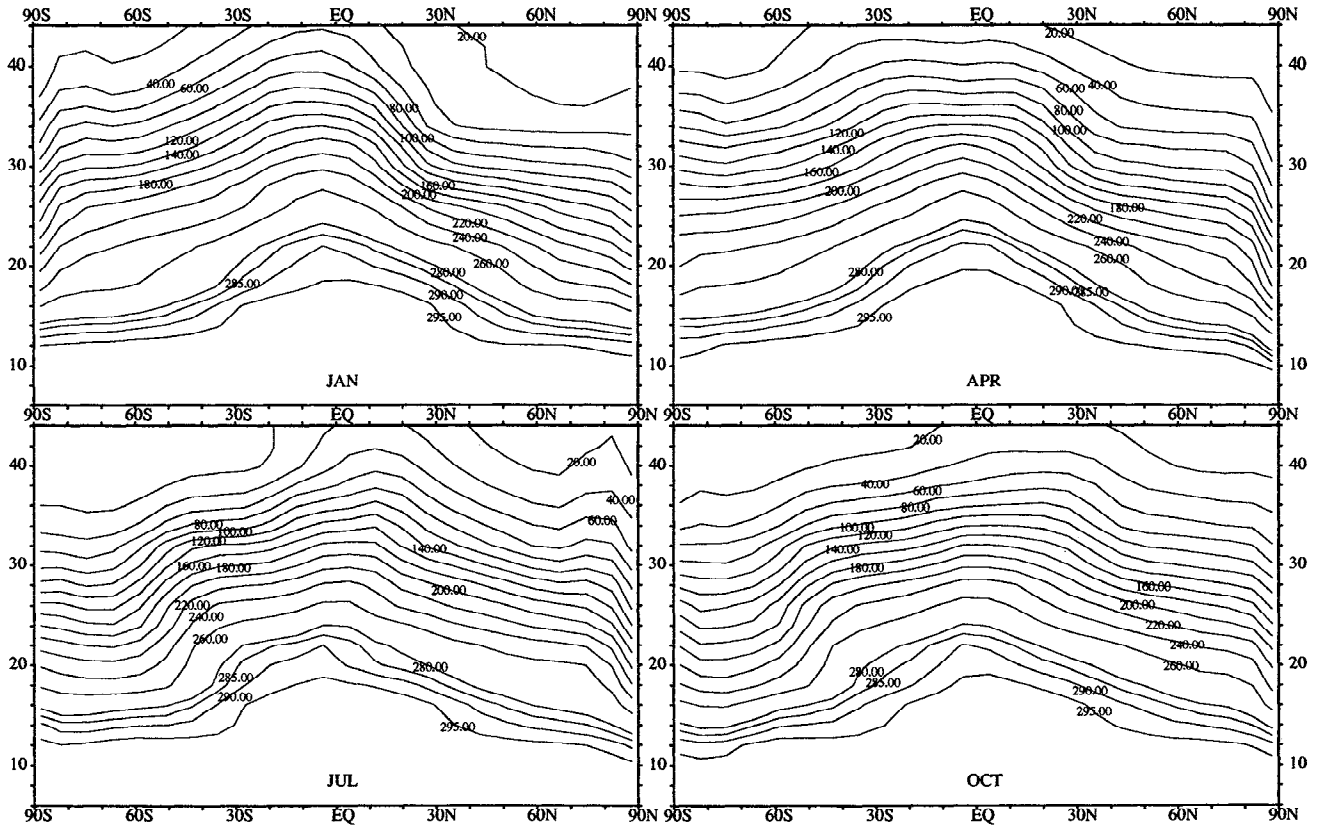


**Figure 1.** Zonal-mean $N_2O$ concentration from the CTM averaged over the months January, April, July, and October, as labeled. Contours are labeled in parts per billion.

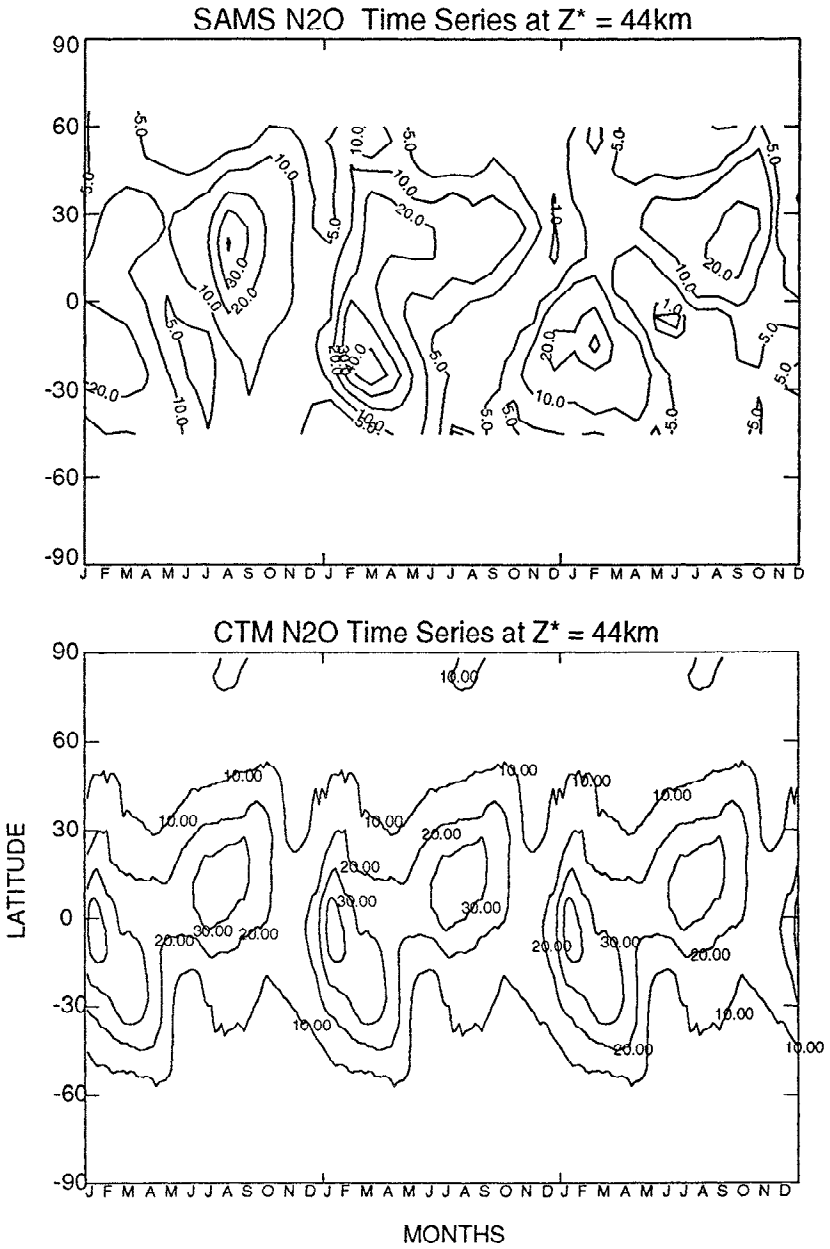


**Figure 2.** Latitude versus time of zonal-mean $N_2O$ concentration. (Top) SAMS observations for 1979–1981; (bottom) model year repeated 3 times. The altitude for both is 44 km. Contours are labeled in parts per billion.

peaks in modeled concentrations remain about 10° too close to the equator in both hemispheres. The CTM is in similar agreement with SAMS at 36 km (not shown); here model peak values are slightly smaller than SAMS (120 ppb compared to 140 ppb), as are the midlatitude values (60 ppb compared to 70 ppb).

Comparing with climatic mean patterns at northern winter latitudes from aircraft observations [*Podolske et al.*, 1993], the model predicts the large winter descent over the poles, matches the slopes of the $N_2O$ contours in latitude-pressure coordinates, but is consistently high by about 20 ppb at 16 km (100 mbar) increasing to 40 ppb at 21 km (50 mbar). A resolution of this discrepancy would require compression of the contours between 12 and 20 km with a corresponding expansion between 22 and 32 km in order to maintain agreement with SAMS. Such a shift would imply a greater barrier to vertical transport below 20 km than in the current model and is not inconsistent with the $CO_2$ profile data (see Figure 3 of *Hall and Prather* [1993]).

## Ozone

The $O_3$ simulations have been described by *Prather et al.* [1990a], who documented the seasonal cycle in column ozone abundance. Here we focus on transport in the lower stratosphere and examine the $O_3$ distribution across the tropopause. In Figure 3 we compare zonal-mean modeled $O_3$ concentrations (lines) to a cli-

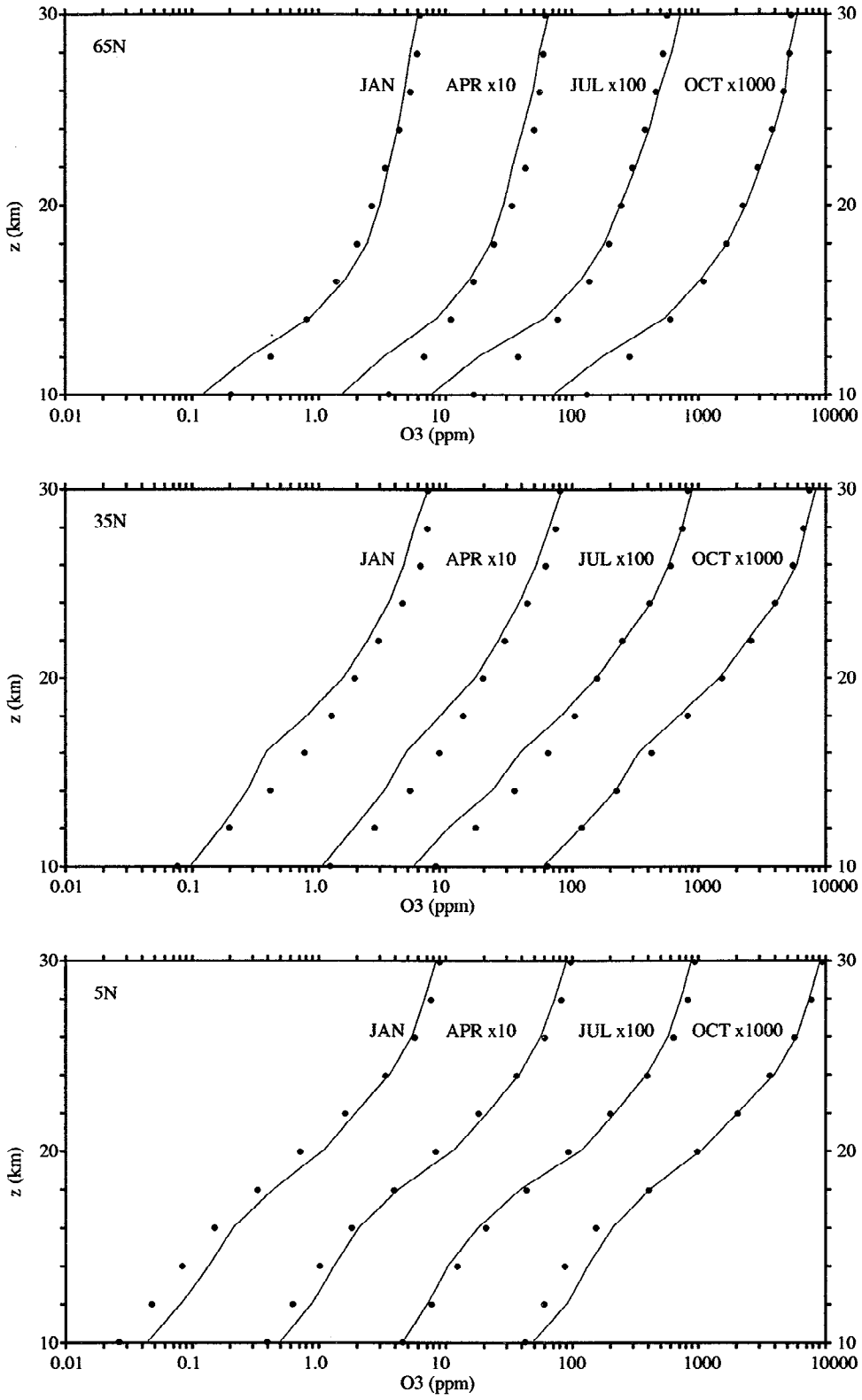


**Figure 3.** Zonal-mean profiles of SBUV (points) and modeled $O_3$ concentration (lines) for the monthly means of January, April, July, and October. The different panels correspond to the latitudes 5°N, 35°N, and 65°N as labeled. The horizontal axes are logarithmic in the $O_3$ concentration, and individual profiles are displaced by factors of 10, as labeled, for clarity.

matic mean (points) developed from Nimbus 7 Solar Backscatter Ultraviolet (SBUV) and the Stratospheric Aerosol and Gas Experiment II (SAGE II) observations [*McPeters*, 1993]. Vertical profiles are shown at three northern latitudes (5°N, 35°N, and 65°N) for each of four months (January, April, July, and October). Basic agreement is good, although our simplified lower boundary condition and lack of tropospheric ozone chemistry makes these comparisons less useful in the upper troposphere. The most important fact is that the sharp vertical gradient of $O_3$ through the lower stratosphere and across the tropopause is well represented in these simulations.

## 4. Tracer Correlations: $CO_2$–$N_2O$

In this section we analyze the simulated $CO_2$–$N_2O$ relationships which are summarized graphically by plotting one trace gas concentration against the other. These "scatterplots" often display compact, smoothly varying features called "correlation curves." In the $CO_2$ plots shown here we have compensated for the regular increase in $CO_2$ concentrations (1.5 ppm/yr in the troposphere in these simulations) by linearly shifting values to a common reference time, preserving seasonal variations. The first subsection describes our realistic simulations of $CO_2$ and $N_2O$ and demonstrates the large seasonal and spatial variations in both shape and compactness of the correlation curves. In order to understand the mechanisms responsible for these departures from a single universal curve, the second subsection analyzes results from simulations of several hypothetical tracers: (1) a tracer like $CO_2$, but driven only by a smooth linear increase in time, and (2) three tracers like $N_2O$, but each with a different, highly simplified form of stratospheric loss. This section concludes with discussion of selected $CO_2$–$N_2O$ observations.

### Realistic $CO_2$–$N_2O$ Simulations

Figure 4 is a comprehensive scatterplot displaying modeled $CO_2$ and $N_2O$ mixing ratios (dots) sampled every 2 km in pressure altitude from 6 to 44 km, every 5 days, every 10° in longitude, at 44°N (measurements, the large symbols, are discussed later). To a first approximation, the points are concentrated in a narrow band relative to the range of values (0–300 ppb for $N_2O$ and 343–353 ppm for $CO_2$), which defines a smooth curve. To second order we note scatter about this curve that has distinctive patterns at different $N_2O$ values.

This first approximation can be understood in terms of the *Plumb and Ko* [1992] theory of tracer correlations.

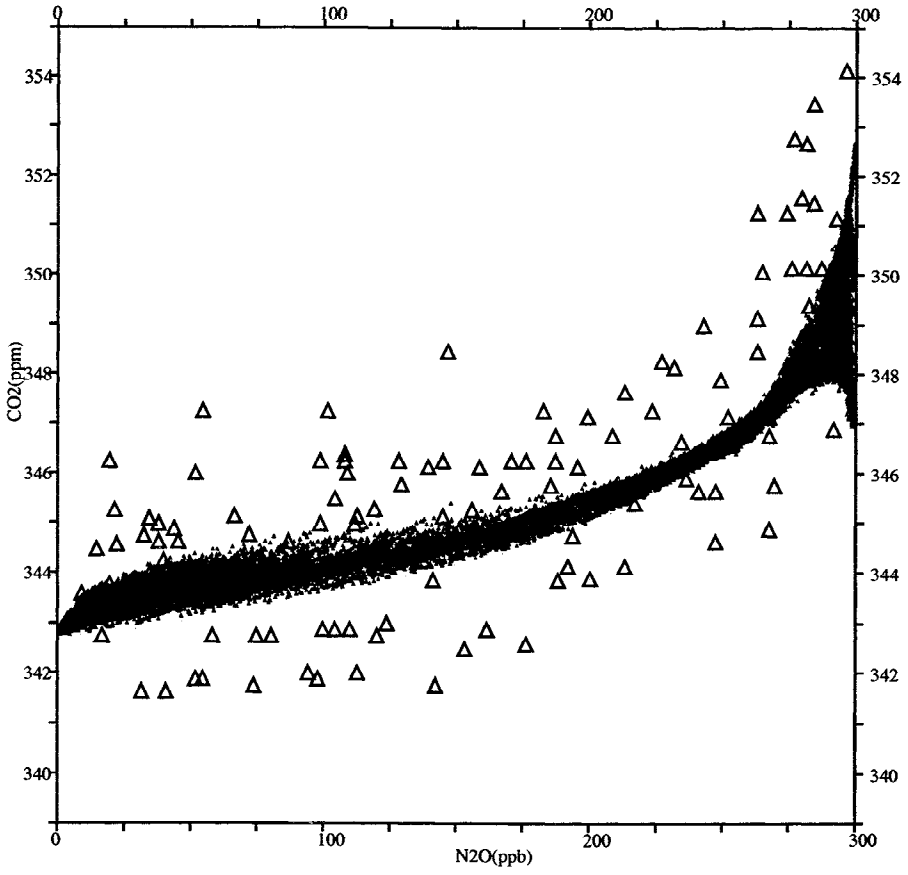


**Figure 4.** Modeled $CO_2$ versus $N_2O$ instantaneously every 5 days (for a full year), every 10° longitude, every 2 km pressure altitude from 6 to 44 km, at 44°N (points). Also shown (triangles) are data from 10 years of balloon soundings *Schmidt et al.*, 1991.

A trace gas is in the "slope-equilibrium" limit in the lower stratosphere when all its chemical processes and time variations are negligibly slow compared to wave-induced quasi-isentropic mixing. Such tracers have isopleths conforming to a common shape, with a downward slope from low to high latitudes determined by the balance between the rapid quasi-horizontal mixing along isentropes and the slower Brewer-Dobson mass circulation [*Holton*, 1986]. When two trace gases have parallel isopleths, the concentration of one uniquely determines that of the other, their fluctuations are correlated, and the scatterplots form compact, universal curves.

The relationship between $N_2O$ and $CO_2$ does not fit this approximation perfectly. In the lower stratosphere ($N_2O > 275$ ppb in Figure 4) a major reason is the annual cycle in $CO_2$, which we shall show produces significant seasonal variations in the shape of the $N_2O$–$CO_2$ correlation curve and, in particular, the scatter about the curve. The presence of scatter indicates that $CO_2$ seasonal variations, which enter the stratosphere in the tropics, are too rapid to be homogenized on mixing surfaces (isentropes); thus the relative slope of $CO_2$ and $N_2O$ surfaces changes seasonally. Similarly, on mixing surfaces in the upper stratosphere, the photochemical loss of $N_2O$ is too rapid in the tropics for its effects to be evenly distributed. In the upper stratosphere $CO_2$ and $N_2O$ surfaces are also not parallel, producing the scatter about the curve at $N_2O$ concentrations below

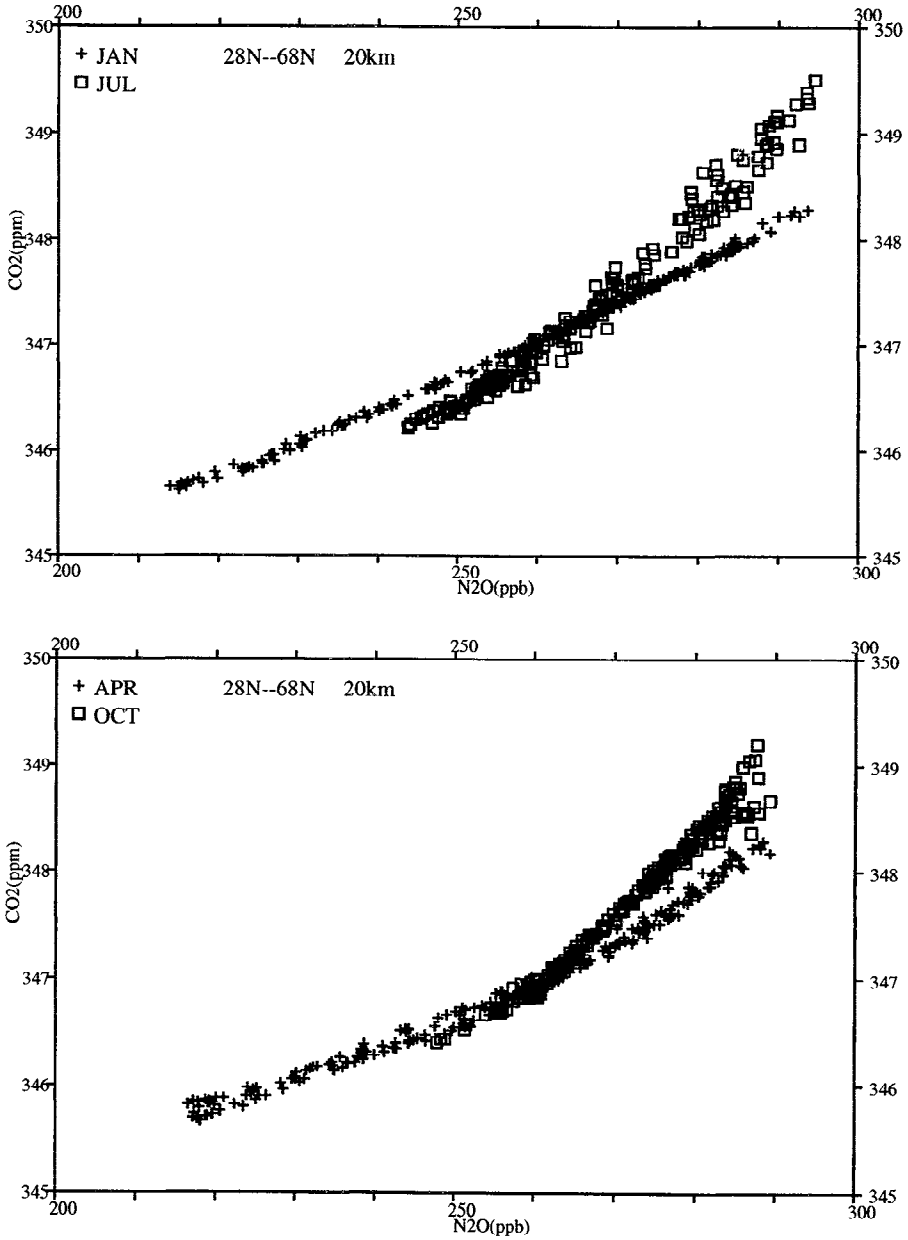


**Figure 5.** Modeled $CO_2$ versus $N_2O$ every 10° longitude, every 8° latitude from 28°N to 68°N and a pressure altitude of 20 km. The top panel shows January 1 and July 1 and the bottom panel, April 1 and October 1.

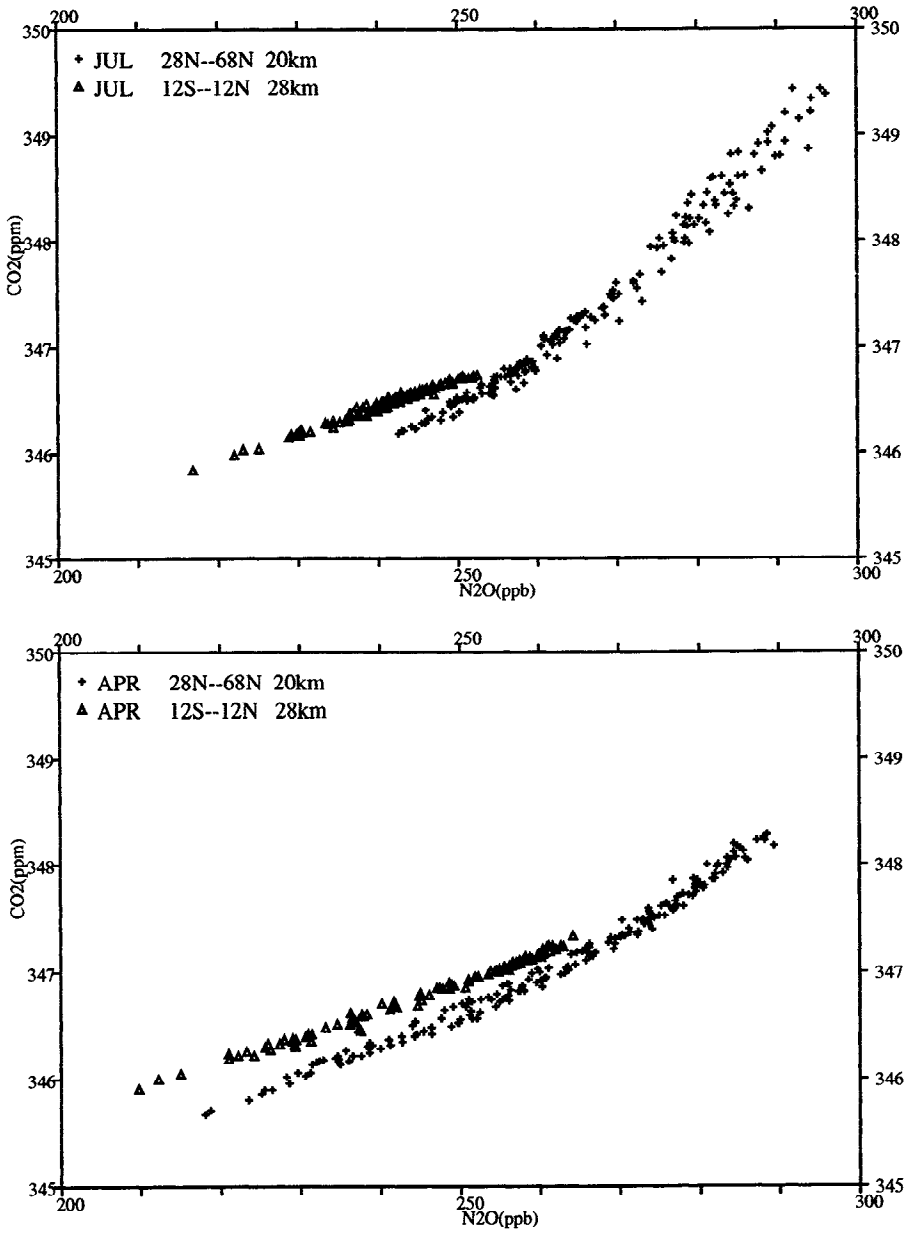


**Figure 6.** Triangles are modeled $CO_2$ versus $N_2O$ every 10° longitude, from 12°S to 12°N, and pressure altitude of 28 km. Crosses are every 8° latitude from 28°N to 68°N and a pressure altitude of 20 km. Both curves in the top panel are July 1, and the bottom panel April 1.

about 150 ppb in Figure 4. In between 150 and 275 ppb there is less scatter.

For a sampling strategy motivated by typical flight paths of research aircraft in the lower stratosphere, Figure 5 displays instantaneous concentrations of $CO_2$ versus $N_2O$ in January, April, July, and October. Values are plotted at 20 km pressure altitude for every 10° longitude and 8° latitude (28°N to 68°N). Significant seasonal features of the correlation curves are (1) lower values of $N_2O$ sampled in winter, reflecting the descent of high-latitude air; (2) more scatter in July, possibly due to slower quasi-horizontal mixing in summer; and (3) a large increase of slope from January to July (because of the annual cycle, the latitudinal $CO_2$ gradient at 20 km peaks in summer, and thus the largest $CO_2$ range is sampled for the same range of $N_2O$).

The tracer-tracer curves do not change slope uniformly throughout the stratosphere. As a clear example of the lack of universality, a high-altitude tropical sampling (28 km, every 10° longitude, every 8° latitude from 12°S to 12°N) is superimposed in Figure 6 on the same midlatitude July and April curves shown in Figure 5. For the same range of $N_2O$ values in both seasons there is an obvious discontinuity between the tropical and midlatitude curves. This is a consequence of the smaller annual $CO_2$ cycle at 50 ppb of $N_2O$ in the tropics than in high latitudes where the same $N_2O$ mixing ratios occur at lower altitudes, and it represents

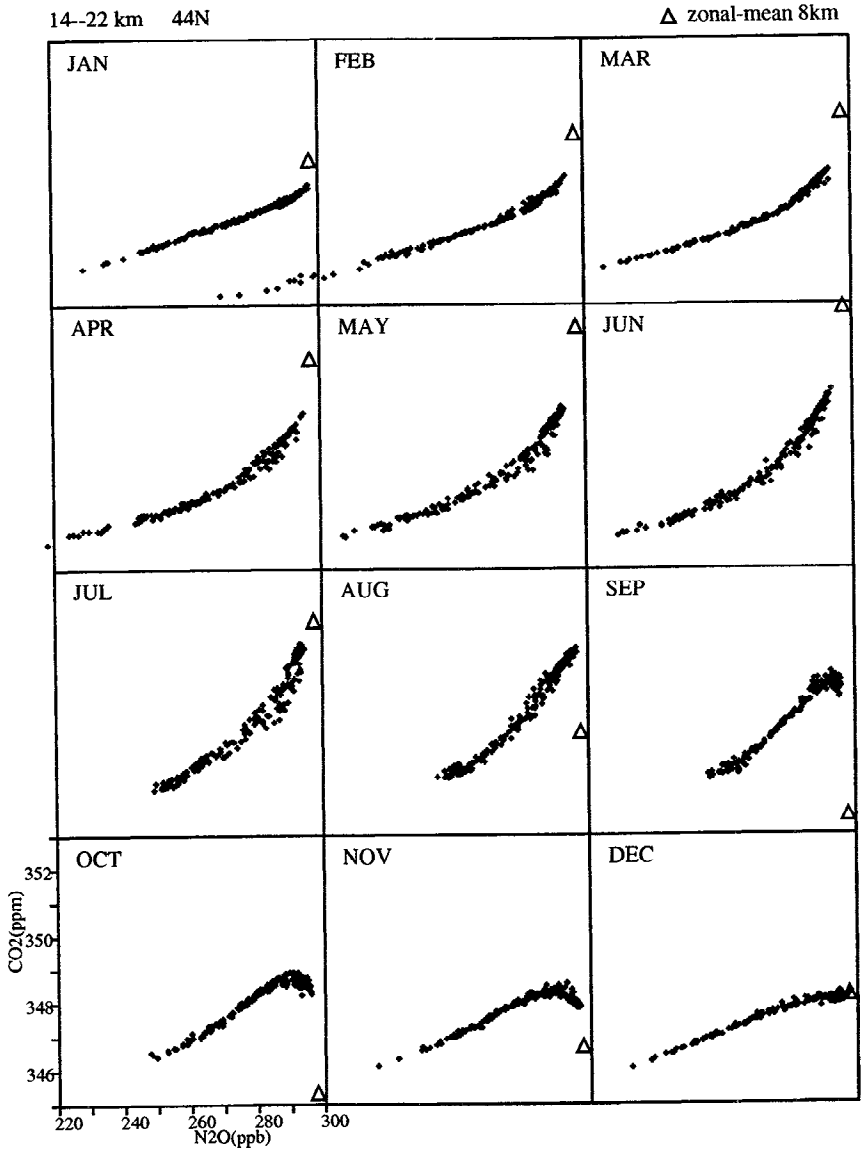


**Figure 7.** Modeled $CO_2$ versus $N_2O$ for the first day of each month of the year. Points are plotted for every 10° longitude, every 2 km pressure altitude from 14 to 22 km, and a latitude of 44°N. The large triangles represent the zonal-mean values at 44°N and 8 km.

a departure from a universal form for the $N_2O$–$CO_2$ relationship.

It is necessary to cut across pressure altitudes to see the reversal of the $N_2O$–$CO_2$ curve observed during certain times of year [*Boering et al.*, 1994]. For example, Figure 7 shows plots for the first day of each month at 44°N, every 10° in longitude, every 2 km in pressure altitude from 14 to 22 km (a sampling strategy analogous to aircraft "dives"). Minimum $N_2O$ values occur in February, a result of high-latitude winter descent of air. In September, October, and November, the slope of the curve reverses, becoming negative for $N_2O$ between 285 and 300 ppb. Evidently, in both the model and real atmosphere the annual $CO_2$ cycle in the midlatitude lower stratosphere is strong enough for its gradients in the northern autumn to more than cancel the gradients forced by the steady trend alone. As a consequence, $CO_2$ in this region increases vertically with altitude, and the correlation curve with $N_2O$ has a negative slope.

Also shown in Figure 7 is the zonal-mean $N_2O$–$CO_2$ point at 44°N and 8 km. The large-amplitude attenuation (see also Figure 4 of *Hall and Prather* [1993]) and the 6-week phase shift of the annual cycle from 8 to 14 km at 44°N reflects the slow rate of direct vertical transport from the upper troposphere to lower stratosphere at midlatitudes. The abrupt phase variation across the tropopause is shown in Figure 8, a plot of the zonal-mean phase versus height from the upper troposphere through the lower stratosphere at 44°N and 4°N. In the troposphere the phase has little height variation, and the signal at midlatitude leads the tropics. In the stratosphere the phase lags rapidly with height, and the tropics lead the midlatitudes. This implies prop-

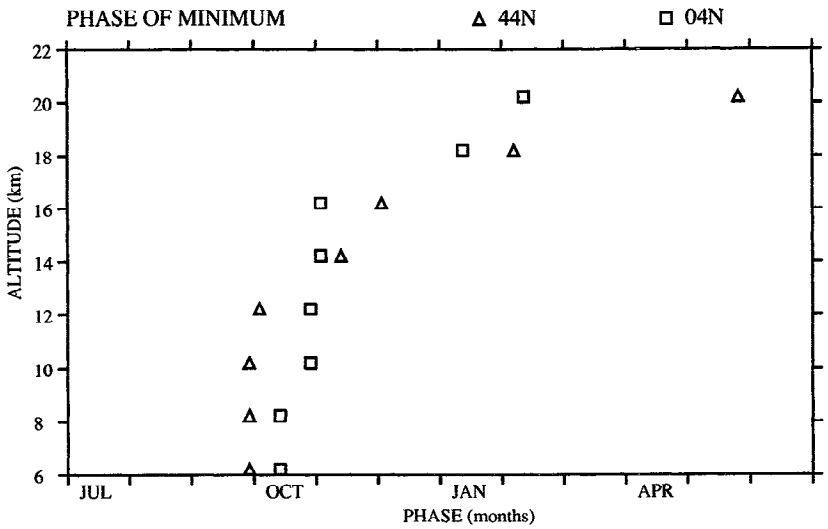


**Figure 8.** The phase of the minimum in the modeled $CO_2$ annual cycle as a function of pressure altitude. Triangles represent 44°N and squares 4°N.

agation from mid to low latitudes in the upper troposphere, through the tropopause in the tropics, and back to midlatitudes in the lower stratosphere.

## $CO_2^T$–$N_2O$

We wish to reduce $CO_2$ to a strictly chronological tracer, so that the difference between stratospheric and tropospheric concentration is a direct measure of the age of stratospheric air (i.e., the average elapsed time since air entered the stratosphere). Thus we simulate a hypothetical tracer, called $CO_2^T$, driven only by the regular tropospheric trend of 1.5 ppm/yr; there is no seasonally varying component. As with $CO_2$, when plotting $CO_2^T$ concentrations from different times on the same graph we compensate for the regular 1.5 ppm/yr increase in concentrations by a linear shift to a common reference time.

Figure 9 shows instantaneous $N_2O$–$CO_2^T$ in January, April, July, and October at 20 km, for every 10° longitude, and every 8° latitude from 28°N to 68°N, the same sampling strategy as the $N_2O$–$CO_2$ plot of Figure 5. Compared to the $N_2O$–$CO_2$ curves, the January and July curves of $N_2O$-$CO_2^T$ are nearly coincident. Thus much of the variation of curve shape for $N_2O$–$CO_2$ is due to the $CO_2$ annual cycle.

In Figure 10 we plot $CO_2^T$ versus $N_2O$ by sampling the model stratosphere at 12°, every 10° longitude, at four pressure altitudes (16, 18, 20, and 22 km as indicated by the symbols) on the first day of each month. The curves show seasonal changes. In June and July there is significant banded structure: the points on one pressure level fall on straight lines which are displaced from the lines of adjacent levels. The slope of the correlation curve is steeper when sampling vertically (band-to-band) than horizontally (within a band). Similar banded structure occurs in the upper stratosphere, as shown in Figure 11, but in this case the mean slope from altitude to altitude is almost flat, whereas the longitudinal sampling (presumably planetary waves acting on meridional gradients) is steep. This clear dependence on sampling direction violates the universality of tracer-tracer correlation curves predicted by the slope-equilibrium analysis of *Plumb and Ko* [1992].

To establish the connection between the sampling strategy and the shape of correlation curves, consider a probe moving in a latitude-altitude plane of the atmosphere with a specified path of slope $m_{\text{path}} = (dz/dy)_{\text{path}}$ in Cartesian coordinates ($z$ and $y$ in kilometers of pressure altitude and latitude). Along its path the probe makes measurements of two tracers with mixing ratios $f$ and $g$. A surface of constant $f$ intersecting the plane forms a line of slope

$$m_f = \left(\frac{dz}{dy}\right)_f = \frac{\partial f/\partial y}{\partial f/\partial z} \tag{7}$$

and likewise for $g$. Let $\delta f$ and $\delta g$ be incremental changes in the tracer measurements along the probe path. One can show that the corresponding slope $\mu_{\text{path}}(f, g)$ in the $f - g$ correlation curve is

$$\mu_{\text{path}}(f, g) = \frac{\delta f}{\delta g} = \frac{\partial f/\partial z}{\partial g/\partial z}\left(\frac{m_{\text{path}} + m_f}{m_{\text{path}} + m_g}\right) \tag{8}$$

Note that when tracer isopleths are parallel ($m_f = m_g$), the slope of the correlation curve is independent of the probe path. However, if the shape of the isopleths of $f$ and $g$ differ, the $f$–$g$ curve will vary with the direction of sampling. Most trace gases have isopleths of shallow slope, and most realistic sampling strategies have vertical components. Therefore usually $m_{\text{path}} \gg m_{f,g}$, and the slope of the $f$–$g$ curve is approximately the ratio of the vertical gradients. For a purely horizontal path (constant pressure altitude $z$), the slope varies as $m_f/m_g$.

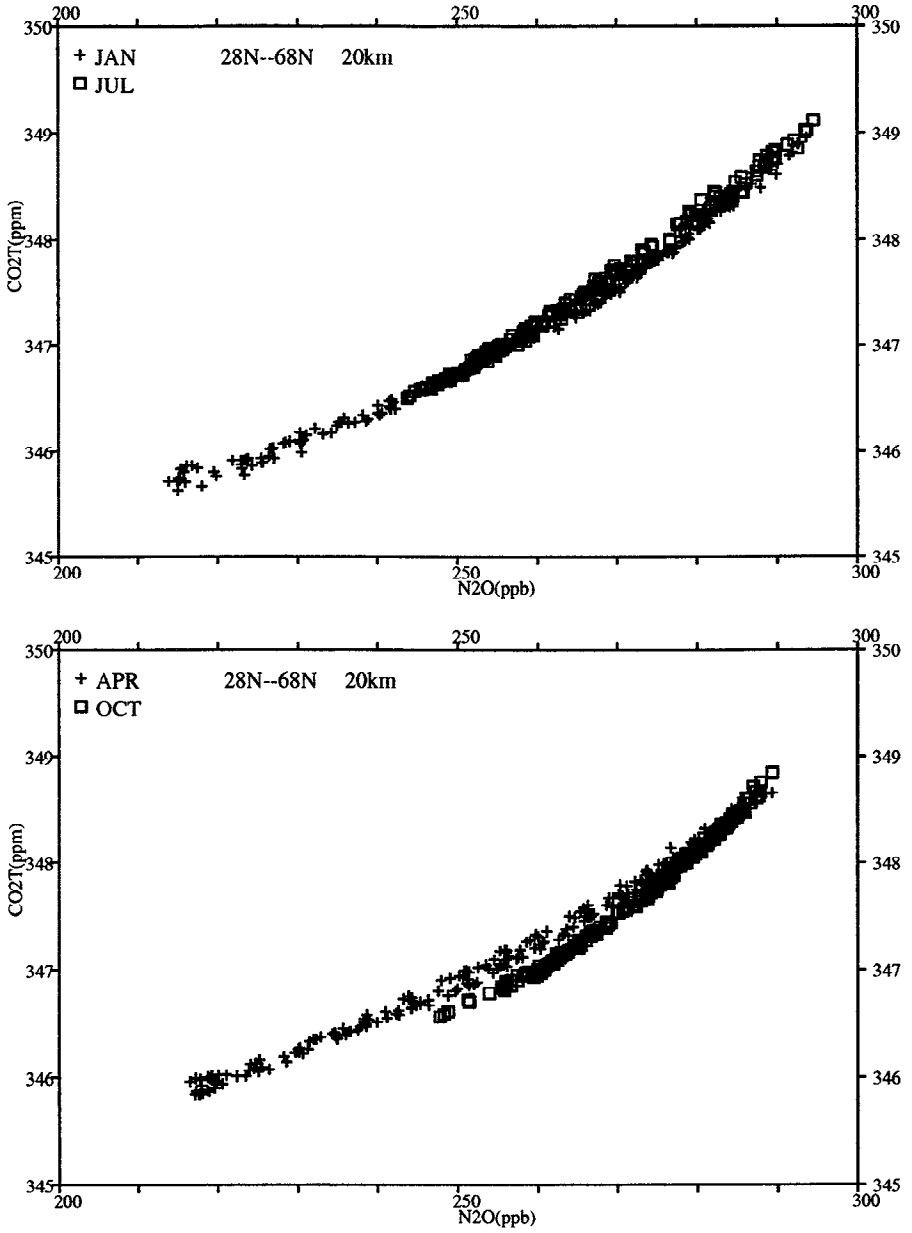


**Figure 9.** Modeled $CO_2^T$ versus $N_2O$ every 10° longitude, every 8° latitude from 28°N to 68°N and a pressure altitude of 20 km. The top panel shows January 1 and July 1 and the bottom panel, April 1 and October 1. This figure is identical to Figure 5, but with $CO_2^T$ replacing $CO_2$.

The slopes of the isopleths for $N_2O$ and $CO_2^T$ in latitude-pressure coordinates are shown in Figures 12 and 13. In these figures we have averaged all longitudes over a year. To first order the two tracers display the same qualitative structure: bulging up in the tropics and sloping down toward either pole. A more detailed comparison reveals that at midlatitudes the $N_2O$ isopleths are less steep than those of $CO_2^T$ in the upper stratosphere, but more steep in the lower stratosphere (i.e., for $N_2O > 260$ ppb).

The relative slopes of these isopleths are equivalent to the spatial variation of the slopes of the tracer-tracer correlation curves. At midlatitudes in the upper stratosphere, $|m_{CO_2}| > |m_{N_2O}|$ and consequently $\mu_{horiz} > \mu_{vert}$ (see equation (8)), whereas in the lower stratosphere $|m_{CO_2}| < |m_{N_2O}|$ and $\mu_{horiz} < \mu_{vert}$. The isopleth shapes can be understood as chemistry interacting with the meridional mass circulation of the stratosphere [e.g., *Holton*, 1986; *Plumb and Ko*, 1992]. Atmospheric gradients of $CO_2^T$ are caused by the steady increase in concentration at the surface carried into the stratosphere by equatorial upwelling and mixed to higher latitudes by quasi-horizontal diffusive mixing. $N_2O$ gradients are driven by the rapid photochemical destruction in the upper stratosphere. Nevertheless, its isopleths show structure similar to $CO_2^T$, as ascent in the tropics brings $N_2O$-replenished tropospheric air to the upper stratosphere, and descent at high latitudes brings

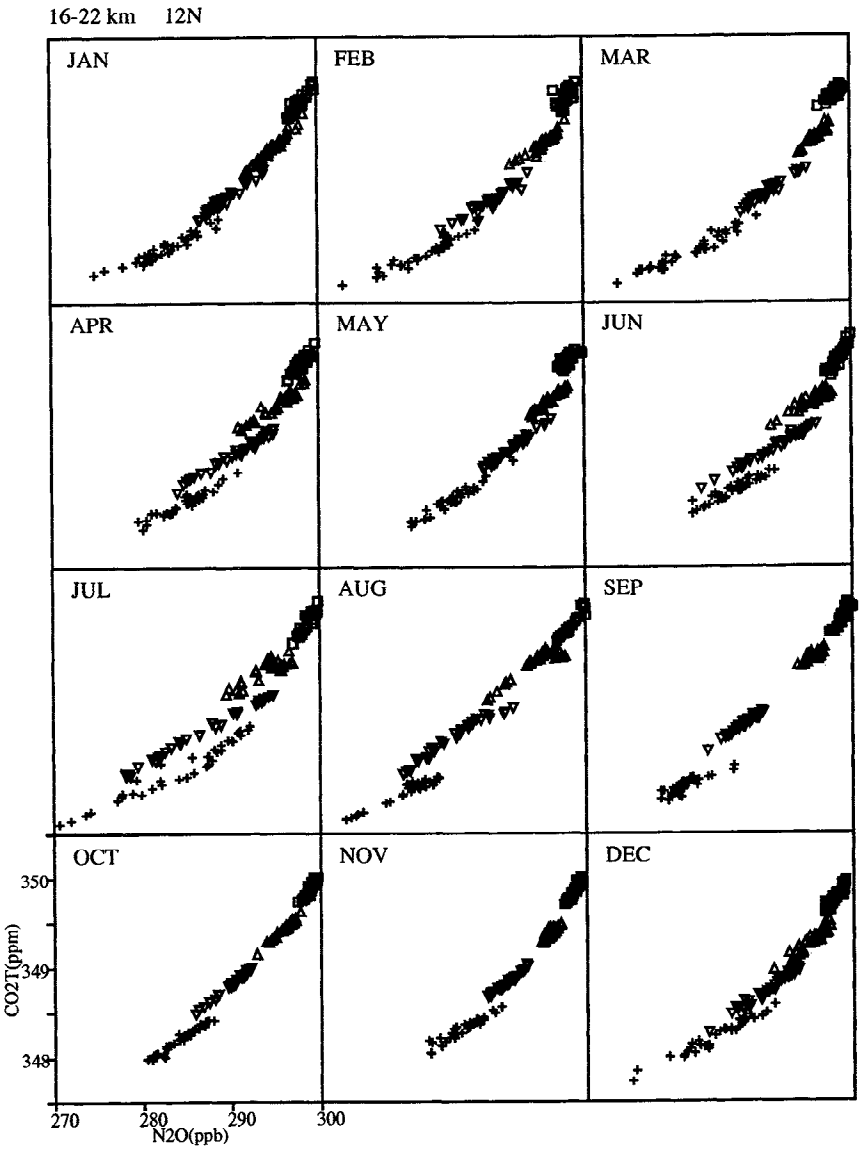


**Figure 10.** $CO_2^T$ versus $N_2O$ for the first day of each month. All longitudes are plotted. The latitude is 12°N, and the altitudes are 16 km (squares), 18 km (up triangles), 20 km (down triangles), and 22 km (pluses).

$N_2O$-depleted air to the lower stratosphere. However, the rapid photochemistry aloft flattens $N_2O$ isopleths relative to $CO_2^T$ in the upper stratosphere, and the $N_2O$-depleted air descending at high latitudes steepens them relative to $CO_2^T$ in the lower stratosphere.

Three hypothetical $N_2O$-like tracers are simulated by the CTM to ascertain which properties of the stratospheric chemical loss are responsible for these $N_2O$–$CO_2^T$ patterns. The most obvious property of the $N_2O$ loss frequency $L$ is the increase with altitude. We approximate this property with the simple formulation

$$\begin{aligned} L(p) &= 0 && p > 100 \text{ mbar} \\ L(p) &= 3 \times 10^{-6}\left(\tfrac{1 \text{ mbar}}{p^2}\right) \text{ s}^{-1} && 1 \le p \le 100 \text{ mbar} \\ L(p) &= 3 \times 10^{-6} \text{ s}^{-1} && p < 1 \text{ mbar} \end{aligned} \quad (9)$$

used in stratospheric model comparisons [*Jackman et al.*, 1988], eliminating latitudinal and seasonal variations in the chemistry. The zonally and annually averaged isopleths of this tracer, $N_2O^A$, are shown in Figure 14 on top of the $N_2O$ contours. Another question might be how losses in the middle stratosphere impact the isopleths of $N_2O$ in the lower stratosphere. Therefore we define a tracer $N_2O^B$ with no photochemical loss below 48 km (1 mbar) and a uniform loss frequency of (2 weeks)$^{-1}$ above. The zonally and annually averaged isopleths of $N_2O^B$ are shown in Figure 15, also on top of the $N_2O$ contours. As a third example, consider what would happen if the $N_2O$ chemistry were uniform throughout the stratosphere. We define the tracer $N_2O^C$ to have a uniform loss frequency, (20 yr)$^{-1}$, at all altitudes above the 200 mbar (approximately 11 km) level in the CTM. The zonally and annually averaged isopleths of $N_2O^C$ are shown in Figure 16 on top of the $CO_2^T$ contours.

In the upper stratosphere $N_2O$ isopleths slope less steeply toward the poles than those of $CO_2^T$ (Figure 13).

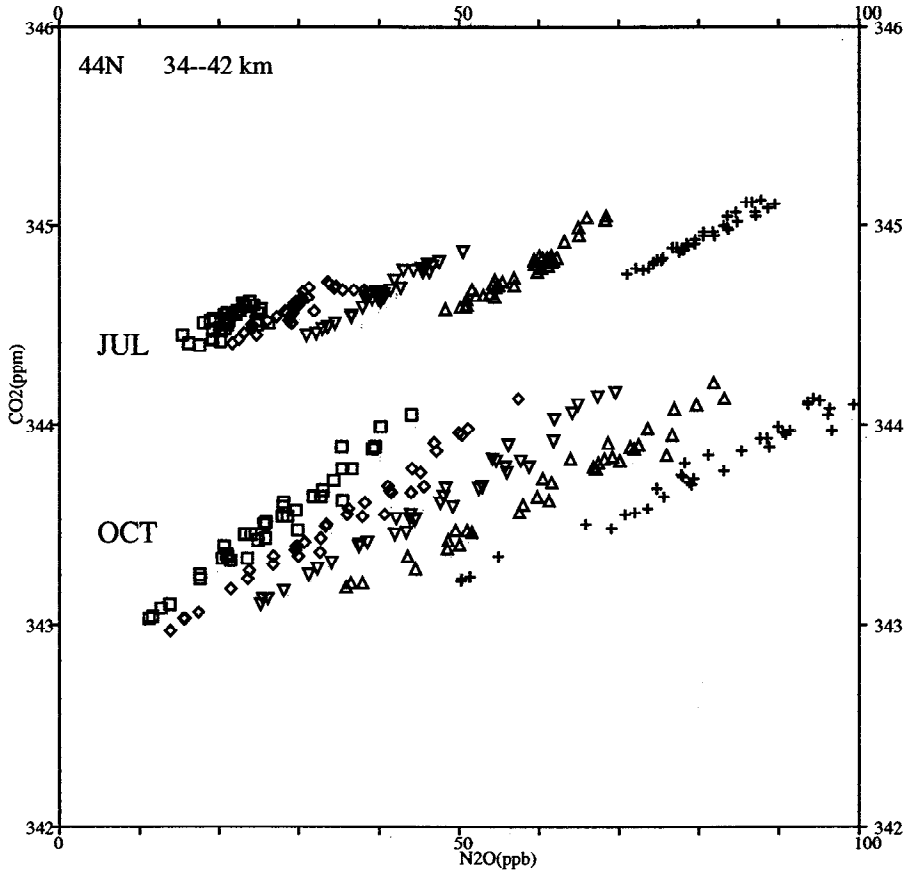


**Figure 11.** $CO_2^T$ versus $N_2O$ in the upper stratosphere. The lower group of points is in October, and the upper, the following July. (Note that this figure is an exception; for the sake of clarity, we have not removed a linear 1.5 ppm/yr trend from October to July.) All longitudes are plotted, the latitude is 44°N, and the altitudes are 34 km (pluses), 36 km (up triangles), 38 km (down triangles), 40 km (diamonds), and 42 km (squares).

On a bulging $CO_2^T$ surface, the photochemical destruction of $N_2O$ is more rapid in the tropics than at high latitudes (which is also at a lower altitude), and losses are too rapid to be homogenized by quasi-horizontal mixing. This effect is seen also for $N_2O^A$, which only has vertical, not latitudinal gradients in chemistry. There is no variation in loss frequency along $CO_2^T$ surfaces for $N_2O^B$ and $N_2O^C$, and these tracers show no tropical suppression relative to $CO_2^T$. Apparently, it is the vertical gradient in photochemistry, rather than latitu-

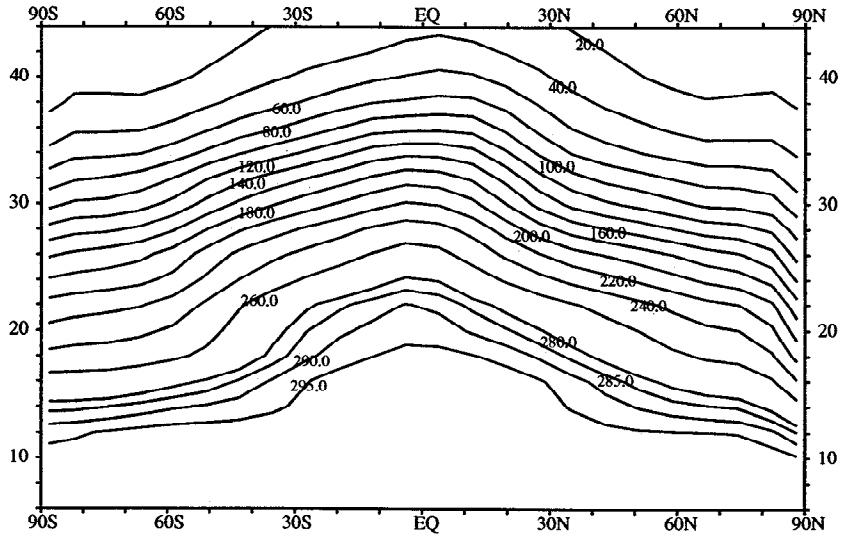


**Figure 12.** Zonal and annual mean contours of modeled $N_2O$. Contours are labeled in parts per billion.

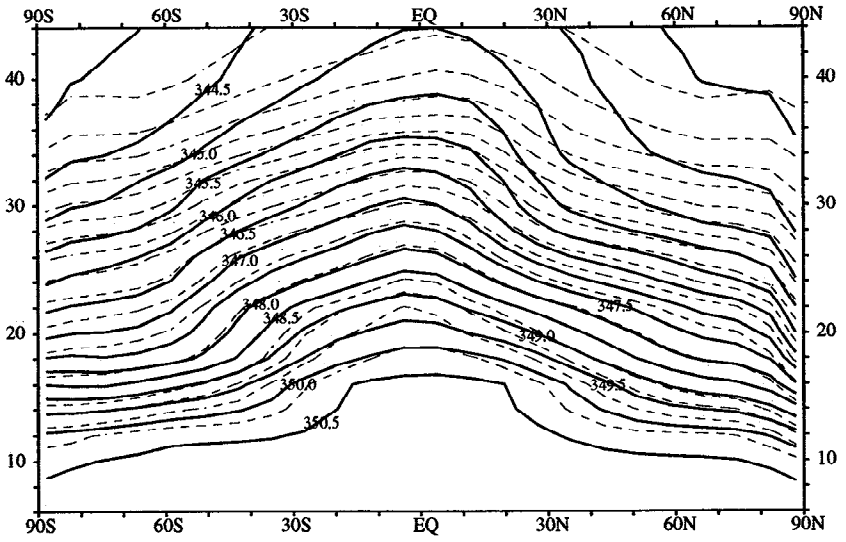


**Figure 13.** Zonal and annual mean contours of $CO_2^T$, labeled in parts per million. The $N_2O$ contours, as labeled in Figure 12, are also shown (dashed lines) for comparison. Note that the $CO_2^T$ isopleths slope more steeply than $N_2O$ at midlatitudes in the upper stratosphere, but less steeply in the lower stratosphere.

dinal, that is primarily responsible for the $N_2O$–$CO_2$ difference in the upper stratosphere.

Even for the case of spatially uniform loss, a tracer will have isopleth shapes more shallow than $CO_2^T$ if its chemical loss is rapid enough. For lifetimes less than about 7 years the tracer mixing ratio is no longer a simple measure of age because the exponential decay cannot be approximated as linear over the spread of ages present in the air parcel (the age spectral width [see *Hall and Plumb*, 1994]). On surfaces of constant age ($CO_2^T$), the width of the age spectrum increases slightly from low to high latitudes [*Hall and Plumb*, 1994]. The additional younger air components present in high-latitude parcels are weighted preferentially by the exponential decay of the tracer, producing isopleth slopes more shallow than those of $CO_2^T$. This effect is negligible for $N_2O^C$ because the loss is too slow. However, it may play some role in flattening $N_2O$ contours relative to $CO_2^T$ in the middle and upper stratosphere.

In the lower stratosphere, Figures 13, 14, and 15 show that isopleths of $N_2O^A$ and $N_2O^B$, like those of $N_2O$, slope downward at midlatitudes more steeply than those of $CO_2^T$. The cause of this difference must be found in transport from the upper stratosphere because $N_2O^B$ has no loss in the lower stratosphere. It must also be due to the increase in chemical loss frequency with altitude because isopleths of $N_2O^C$ (uniform chemistry) line up with those of $CO_2^T$ (Figure 16).

In the midlatitude lower stratosphere, a tracer with a remote source establishes a family of isopleths that

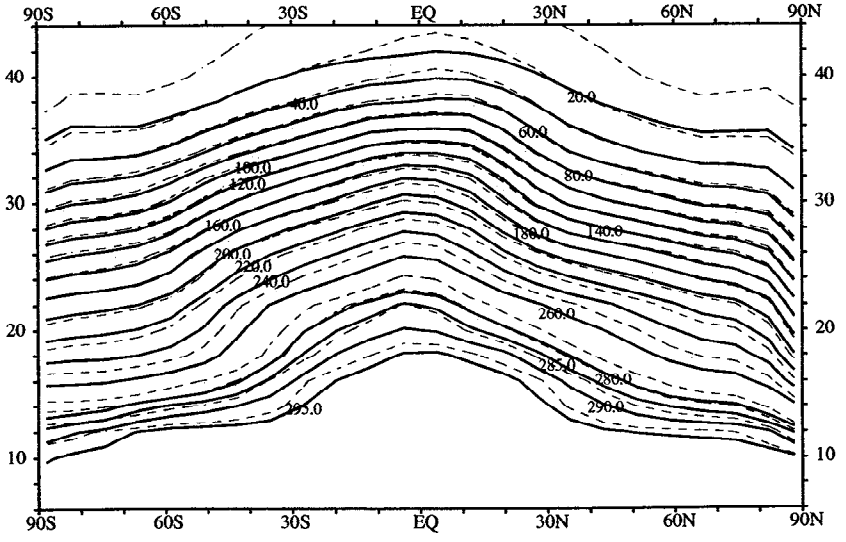


**Figure 14.** Zonal and annual mean contours of $N_2O^A$, a hypothetical tracer with a height-dependent, but latitude- and time-independent, stratospheric photochemical loss rate. Contours are labeled in parts per billion. The $N_2O$ contours, as labeled in Figure 12, are also shown (dashed lines) for comparison.

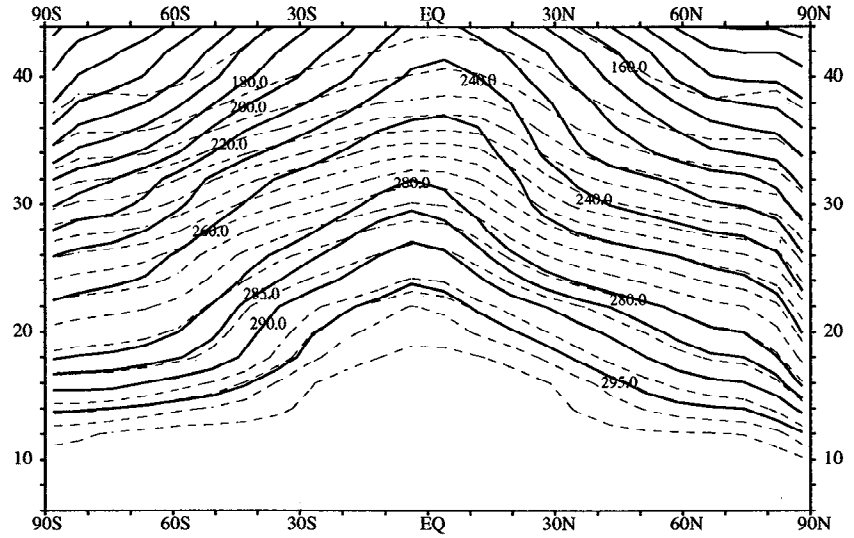


**Figure 15.** Zonal and annual mean contours of $N_2O^B$, a hypothetical tracer with zero photochemical loss at pressure altitudes below the 1 mbar level, and a uniform constant loss rate above. Contours are labeled in parts per billion. The $N_2O$ contours, as labeled in Figure 12, are also shown (dashed lines) for comparison.

slope downward to the poles relative to pressure surfaces. *Holton* [1986] explained the basic shape of these contours. To a first approximation, the isopleths fall along surfaces of rapid adiabatic mixing (i.e., surfaces of constant potential temperature). A tracer on these mixing surfaces, however, can never be homogenized because it is continuously perturbed by a small residual mass flux across these surfaces. On average, air pushes up through the equatorward side of this surface and downward through the poleward side. Thus for a tracer with a vertical gradient at midlatitudes, the isopleths must slope downward to the pole more steeply than the mixing surfaces. This criterion applies to long-lived chemical tracers such as $N_2O$, $N_2O^A$, $N_2O^B$, and $N_2O^C$ and those in the slope-equilibrium limit discussed by *Plumb and Ko* [1992]. It also applies to linearly changing, chronological tracers such as $CO_2^T$.

We have also seen that in the midlatitude lower stratosphere of the model $N_2O$-like tracers ($N_2O$, $N_2O^A$, and $N_2O^B$) have isopleths that slope downward to the poles more steeply than chronological tracers ($CO_2^T$ and $N_2O^C$). Each stratospheric air parcel has a mix of irreducible fluid elements with a range of transit times whose average is defined as the age of the parcel [*Hall and Plumb*, 1994]. (For a linearly increasing tracer, this age is equivalent to the average concentration of

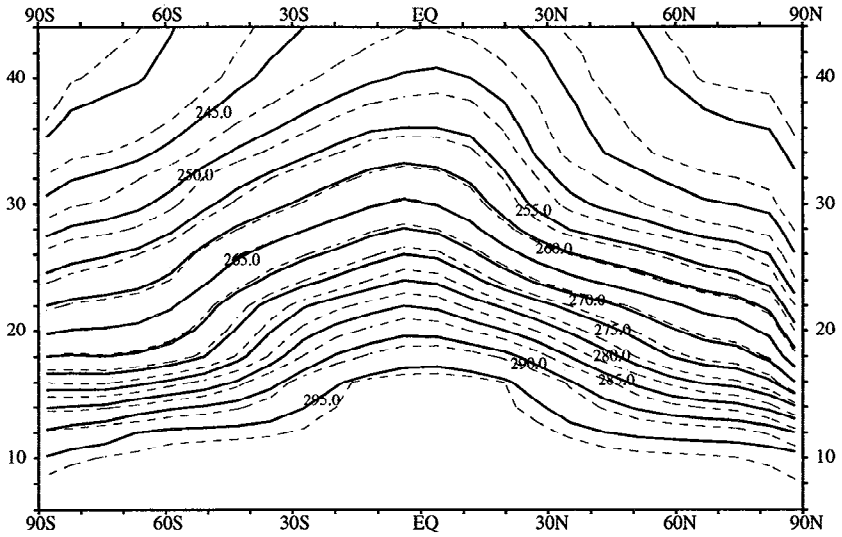


**Figure 16.** Zonal and annual mean contours of $N_2O^C$, a hypothetical tracer with constant uniform photochemical loss at pressure altitudes above the 200 mbar level, and no loss below. Contours are labeled in parts per billion. The $CO_2^T$ contours, as labeled in Figure 13, are also shown (dashed lines) for comparison.

the trace gas.) The mean $CO_2^T$ concentration of a parcel does not depend on the paths of the fluid elements comprising the parcel; however, the concentration of $N_2O$ does. The average photochemical history of parcels along the constant-age surface varies with latitude. For the same transit time since leaving the troposphere, the stratospheric circulation has caused a fluid element on the poleward side of the age surface to traverse higher altitudes on average, and thus have less remaining $N_2O$, than an element on the equatorward side. The integrated photochemical activity along fluid element paths, which can be thought of as a "photochemical age" since elements entered the stratosphere, increases poleward on an age surface for all gases with increasing chemical loss aloft. Thus $N_2O$ (also $N_2O^A$ and $N_2O^B$) isopleths must slope downward to the pole more steeply than those of $CO_2^T$ (also $N_2O^C$). At midlatitudes in the lower stratosphere all such tracers slope more steeply than isentropes, and $N_2O$ tracers slope more steeply than chronological tracers. Thus chronological tracer isopleths are the closest to isentropes.

### $CO_2$–$N_2O$ Observations

Along with the modeled $CO_2$–$N_2O$ scatterplot at midlatitudes, Figure 4 also displays simultaneous measurements of $CO_2$ and $N_2O$ from a decade of balloon soundings in Europe [*Schmidt et al.*, 1991]. To obtain this composite we removed linear trends from $CO_2$ for two different periods, before and after 1987, because of an abrupt, large jump in the $CO_2$ measurements after 1987. In fact, one flight from 1987 was discarded due to excessive scatter, as were three outlier points in the subsequent $N_2O$–$CO_2$ scatterplot. Note that the modeled and observed data have been scaled to a common surface $CO_2$ value. The resulting observations show the same basic structure as the modeled correlation curve: a clear decline in $CO_2$ along with $N_2O$, including some evidence for curvature in this relationship. The observations show large scatter which, in addition to noise, may include effects from interannual variability in both transport and sources, not part of the simulation here. Meaningful model-measurement comparison will require greater precision and more frequent measurements, emphasizing the need for high-resolution aircraft measurements of $CO_2$ in the lower stratosphere [e.g., *Boering et al.*, 1994].

## 5. Tracer Simulations: $O_3$–$N_2O$

Ozone has in general the most rapid photochemistry of the tracers simulated here. In the middle and upper stratosphere, $O_3$ is nearly in local photochemical steady state and has a maximum mixing ratio near 35 km altitude. Because transport plays no direct role in its distribution here, its relationship with long-lived tracers is not compact. In the lower stratosphere, the photochemical timescale for $O_3$ change, defined by either production or loss terms, ranges from a month or two in the tropics to a few years at high latitudes. Thus its global distribution is controlled neither by photochemistry nor by dynamics alone [*Ko et al.*, 1989]. On synoptic scales $O_3$ is a good tracer of atmospheric motions, being correlated with constituents such as $N_2O$ and $NO_y$ [*Murphy et al.*, 1993]. Over larger scales, however, climatic mean surfaces of $O_3$ slope less steeply from equator to pole than those of either $N_2O$ or $CO_2$ (see Figure 17), an effect qualitatively similar to the flattening of upper stratospheric $N_2O$ isopleths. As a result, the shape of the $O_3$–$N_2O$ correlations, even in the lower stratosphere, varies with latitude and altitude more than that of $CO_2$–$N_2O$.

Figure 18 shows how the rapid increase in $O_3$ chemical rates with altitude influences the $O_3$–$N_2O$ correlations. Ozone is plotted against $N_2O$ on July 1, at

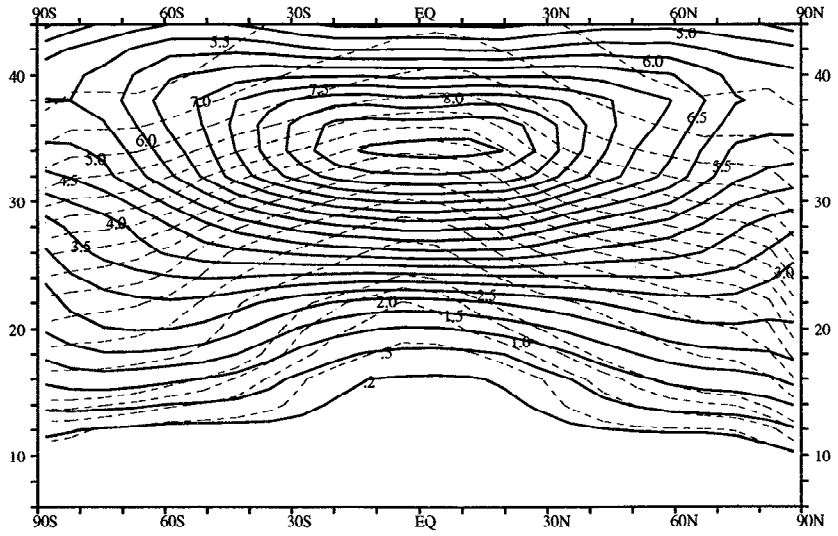


**Figure 17.** Zonal and annual mean contours of modeled $O_3$. Contours are labeled in parts per million. The $N_2O$ contours, as labeled in Figure 12, are also shown (dashed lines) for comparison.

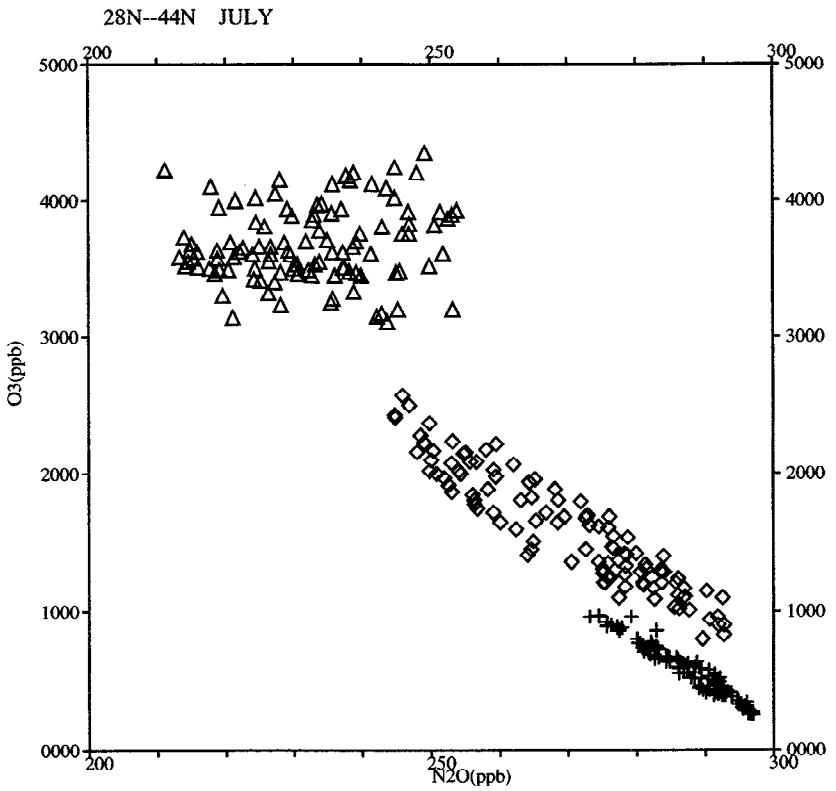


**Figure 18.** Modeled $O_3$ versus $N_2O$ at three altitudes: 16 km (pluses), 20 km (diamonds), and 24 km (up triangles). The latitude range is 28°N to 44°N, and all longitudes are plotted. The time is July 1.

latitudes of 28°N to 44°N, and all longitudes for three different pressure altitudes: 16, 20, and 24 km. At 16 km the two tracers are tightly and negatively correlated. This correlation also holds at 20 km, although there is noticeably more scatter. At 24 km, however, $O_3$ and $N_2O$ are uncorrelated.

In addition to increasing scatter with altitude, the curves fitted through the $O_3$–$N_2O$ correlations for different altitudes are not continuous but form a "banded" structure similar to, but more pronounced than, that of $N_2O$–$CO_2^T$. Note that these bands are a consequence of the particular sampling scheme (i.e., quasi-horizontal at distinct altitudes), and other sampling strategies as described by (7) and (8) would produce different patterns falling within a region of the $O_3$–$N_2O$ diagram, just as the various $N_2O$–$CO_2$ curves differ but fall within the region seen in Figure 4. A vertical profile of $O_3$–$N_2O$ (band-to-band) in general produces a more steeply negative correlation curve than a quasi-horizontal profile (within a band in Figure 18). Similar though less pronounced banded structure occurs in the winter (not shown). Thus a tight correlation between two trace gases can be observed, but this datum cannot be used to infer a similar universal relationship, because a different direction of sampling could change this slope and the scatter about it.

Because $O_3$ isopleths do not coincide with those of $N_2O$, using $N_2O$ as a coordinate system does not remove the dynamically driven variations in $O_3$. Thus in polar regions, large winter descent can bring down air with fundamentally different $O_3$–$N_2O$ correlations. For example, in Figure 19 $O_3$ is plotted versus $N_2O$ on January 1 for all longitudes at midlatitudes (28°N–44°N) and high latitudes (60°N–76°N). The high-latitude slope of the correlation curve is nearly a factor of 3 smaller in magnitude than midlatitudes. Figure 20 shows the concentrations of $O_3$ versus latitude on January 1 for air parcels with $N_2O$ values falling in the range 260±4 ppb (squares) or 230±4 ppb (diamonds). The figure thus represents a latitudinal profile of $O_3$ on the 260 and 230 ppb surfaces of $N_2O$. In addition to the $O_3$ variation at each latitude (in part due to the 8 ppb width of the $N_2O$ band, in part due to sampling regions of different $O_3$–$N_2O$ relationships), there is a transition from 55°N to 65°N, the location of the GCM's stratospheric polar jet, over which the $O_3$ concentration drops about 500 ppb on each $N_2O$ surface. This $O_3$ variation is comparable in magnitude to observations [*Proffitt et al.*, 1990], even though no enhanced polar chemistry is modeled.

These results imply that variations from a predetermined relationship with $N_2O$ cannot unambiguously determine local chemical rates of $O_3$. We agree with *Plumb and Ko* [1992] and question the initial interpretations based on spatial changes in $O_3$ with respect to $N_2O$ observed during the AASE mission [e.g., *Proffitt et al.*, 1990]. Empirical measures of $O_3$ loss based on changes in the $O_3$–$N_2O$ correlations over winter must include measurements of these quantities at all relevant

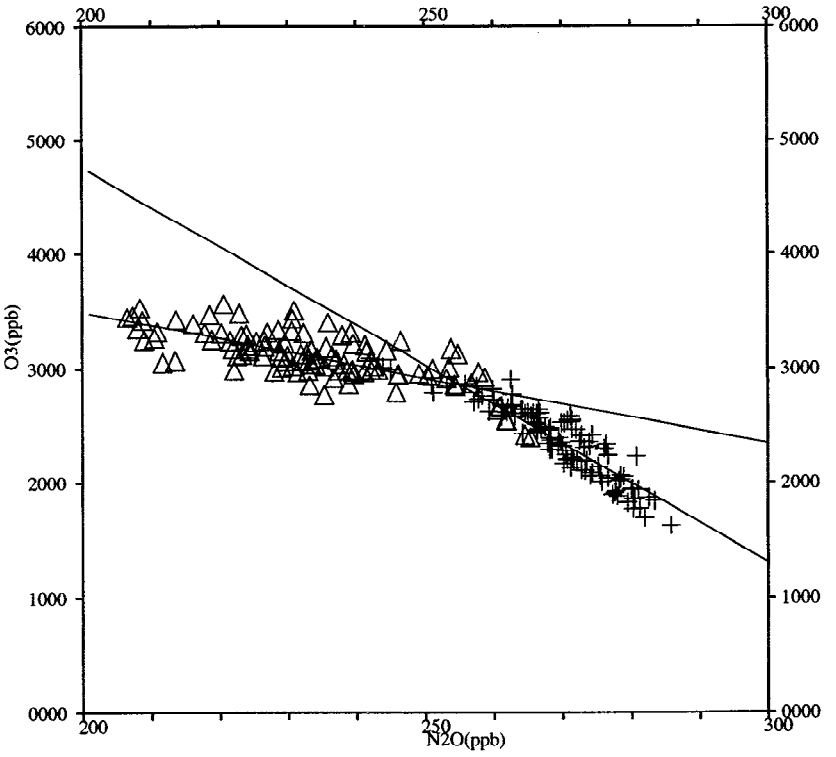


**Figure 19.** Modeled $O_3$ versus $N_2O$ at 22 km on January 1 for all longitudes. The two latitude ranges are 28°N to 44°N (pluses) and 60°N to 76°N (up triangles). Also shown are least squares fit lines for each latitude group. For the midlatitude range $[O_3](ppb)=-23.0[N_2O](ppb)+8211.2$, and for the high-latitude range $[O_3](ppb)=-7.7[N_2O](ppb)+4642.9$. The slope from the midlatitude range is comparable to observations *Proffitt et al.*, 1990, although it depends on the altitude chosen.

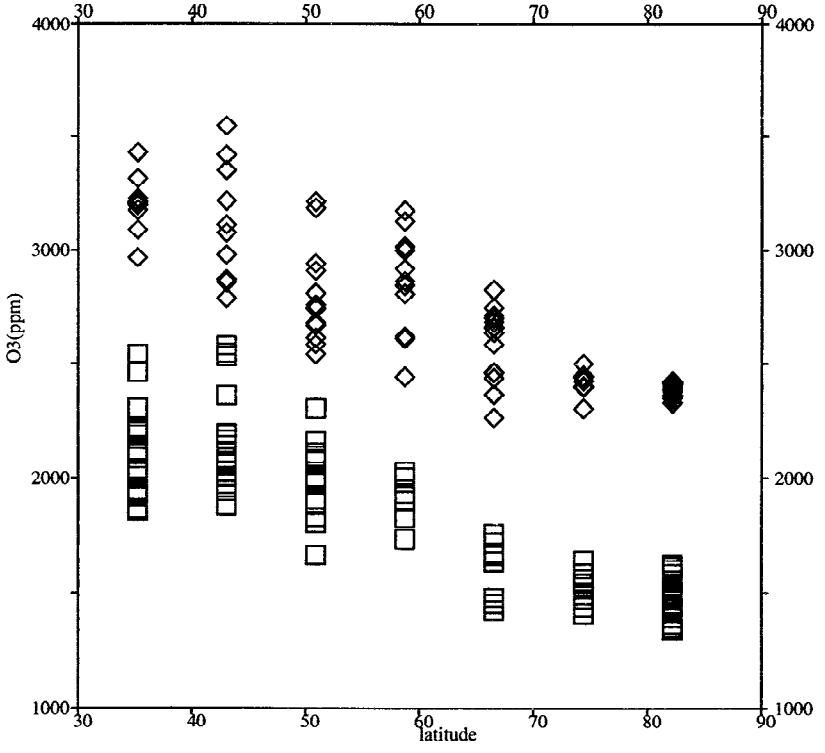


**Figure 20.** Modeled $O_3$ as a function of latitude. $O_3$ concentration is plotted with a square if $N_2O$ in the same grid box has a value between 256 and 264 ppb, and with a diamond if $N_2O$ falls between 226 and 334 ppb. Thus the points form an approximate latitudinal profile of $O_3$ on the 260 and 230 ppb $N_2O$ surfaces. The time is January 1.

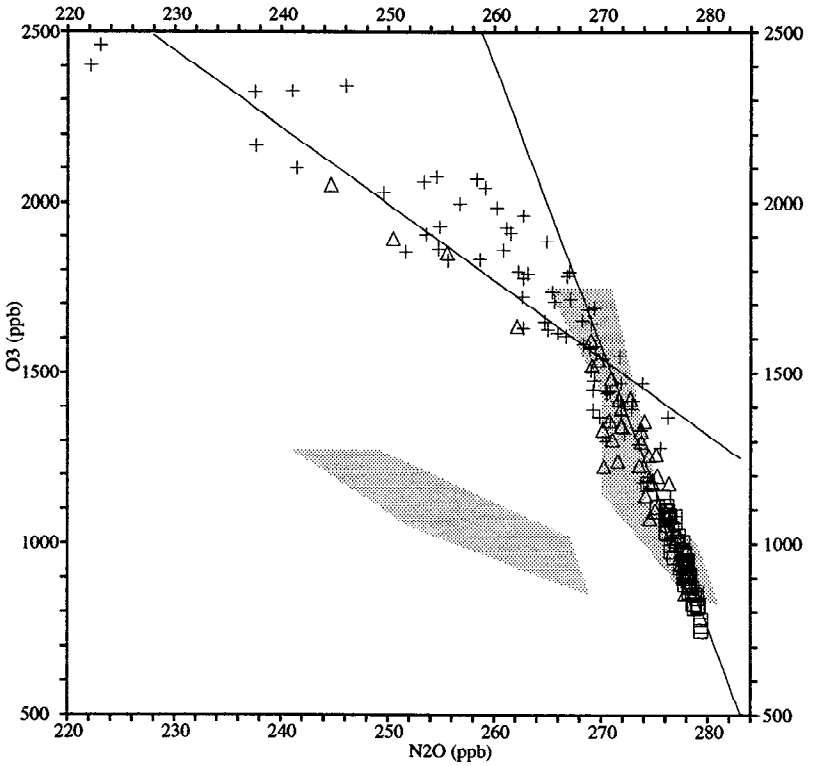


**Figure 21.** Modeled $O_3$ versus $N_2O$ at 20 km on October 1 for all longitudes in three latitude groups: (1) 4°S and 12°S (squares), (2) 20°S (up triangles), and (3) 28°S and 36°S (pluses). Least squares fit lines are shown for groups 1 and 3. The shaded polygons represent approximate regions of the $N_2O$–$O_3$ plane sampled by ER 2 lower stratospheric aircraft flights in the October lower stratosphere *Murphy et al.*, 1993 from 0°S to 15°S (upper right) and 15°S to 30°S (lower left). Modeled $N_2O$ data have been rescaled to match the observations at 280 ppb.

altitudes. Such an analysis is possible, for example, for the region sampled by the DC 8 (10-13 km [e.g., *Collins et al.*, 1993]), when considered with ER 2 observations (15-19 km) which sample the relevant higher-altitude descending air in winter.

A related technique using $N_2O$ to estimate chemical $O_3$ depletion in the winter polar stratosphere assumes $O_3$ and $N_2O$ isopleths are parallel across the polar vortex. From observations of $N_2O$ time trends, *Schoeberl et al.* [1990] deduce an effective vertical velocity dependent on the $N_2O$ zonal mean isopleth slope. Employing observed $O_3$ trends and the $N_2O$-deduced velocity, they estimate the chemical loss necessary to balance the $O_3$ continuity equation. In our model, the $O_3$ slope is less steep than the $N_2O$ slope without any polar chemical loss. To the extent that such a background $O_3$–$N_2O$ relationship is realistic, the magnitude of the *Schoeberl et al.* [1990] downward vertical velocity is overestimated for $O_3$, and thus so is the chemical loss. However, when the evolution of the $O_3$–$N_2O$ relationship is followed through the winter, beginning at high altitude as noted above, this approach should be robust.

In Figure 21 we compare our modeled $O_3$–$N_2O$ correlations to aircraft observations at 15-20 km altitude in low latitudes reported by *Murphy et al.* [1993]. The observations are represented by two shaded polygons (see Figure 7 of *Murphy et al.* [1993] for the individual points). The upper right polygon represents true tropical data (0°S–15°S), and the lower left polygon, the subtropics (15°S to 30°S). The two striking features of the observations are the discontinuous jump in $O_3$ at about 268 ppb of $N_2O$, and the two distinctly different slopes of correlation curve. The modeled $N_2O$–$O_3$ points are sampled at 20 km, all longitude points, for three latitude groups: (1) 0°S and 12°S as squares, (2) 20°S as triangles, and (3) 28°S and 36°S as crosses. In the model there is a transition in the correlation slope from the tropics (group 1) to the extratropics (group 3) nearly as large as the observations; however, the curve is continuous. The observed discontinuity clearly indicates some dynamical barrier to mixing between tropics and subtropics at the time of the observations. The simulation accurately portrays the different chemistries of the two regimes but fails to achieve this dynamical separation. It is not clear what type of circulation would be needed to create the observed pattern.

## 6. Conclusions and Discussion

Simulations of different chemical species in a three-dimensional model provide a means to understand more thoroughly observed trace gas correlations in terms of

different chemistries and large-scale transport. We draw several general conclusions from our results: (1) The slope and degree of compactness for two gases depend, in general, on the sampling strategy, and this must be accounted for when interpreting measurements. (2) Regarding Arctic ozone loss, it is difficult to separate the influence of background structure (i.e., the relative slopes of the isopleths as a function of latitude and altitude) from that of enhanced chemistry when using a long-lived tracer such as $N_2O$ as a coordinate. Defining this background structure, for example using the full set of altitudes covered by the ER 2 and DC 8, should help. (3) The lack of compactness in the observed trace gas correlations contains important information on the chemical and mixing times in the lower stratosphere. Unfortunately, testing the model predictions for $N_2O$–$CO_2$ requires $N_2O$ precision better than 5 ppb, and thus the measurements from the Stratospheric Photochemistry, Aerosols, and Dynamics Expidition (SPADE) [*Boering et al.*, 1994], the most precise to date, may not be suitable.

The third conclusion points to a fundamental measurement of the stratospheric circulation. The relative orientation of the isopleths of two tracers can be obtained directly from the change in the tracer-tracer correlation slope with sampling direction, or equivalently, the spread about the regression line. For species having negligible chemical loss in the lower stratosphere and slowly varying tropospheric sources, the nonuniversality of tracer relationships is a consequence of the finite rate of quasi-horizontal mixing compared to high-latitude descent of "photochemically aged" air, as discussed for $N_2O$–$CO_2^T$. Thus the relative rate of residual advection to horizontal mixing can be obtained from analysis of such correlations. This approach is far more feasible than intensive measurements of individual tracers to determine the mean slope of the isopleths on pressure surfaces, which would require many years of observations to reduce meteorological noise. It is not yet clear which tracers would be optimal for this type of correlation study. Consistent calibration and high precision are vital, although not necessarily high accuracy. Apparently, because of the large influence of the annual cycle in the lower stratosphere, $CO_2$ is not a good choice for illuminating these long term processes below 20 km altitude. However, it likely provides unique information about transport on seasonal time scales and less.

In addition to these general conclusions, there are some specific lessons from the $N_2O$–$CO_2$–$O_3$ studies: (1) The model's maintenance of a reversed vertical gradient in $CO_2$ throughout the autumn in northern midlatitudes agrees with observations [*Boering et al.*, 1994] and demonstrates that only small amounts of tropospheric air enter the stratosphere directly at midlatitudes. (2) The realistic $N_2O$–$O_3$ slopes at low latitudes indicate that the CTM simulates tropical photochemistry well, and in particular, accurately reproduces the relative rates of $O_3$ production to $N_2O$ loss. However, the observed discontinuity between the tropics and subtropics seen in the $O_3$–$N_2O$ observations of *Murphy et al.* [1993] cannot be readily understood with the present model. (3) From both the $CO_2$ and $N_2O$ simulations it appears that the GCM used here mixes air too rapidly into the stratosphere below 20 to 25 km. If both aircraft and SAMS observations of $N_2O$ are consistent, then steeper vertical gradients are required below 20 km with more rapid mixing somewhere above. Clearly, the present model, with 5-km vertical resolution, must be viewed primarily as a didactic tool.

**Acknowledgments.** Initial $N_2O$ simulations were begun at GISS and Columbia University by María M. García. Work at Columbia and UC Irvine was supported by NASA's Atmospheric Chemistry Modeling and Analysis Program and High-Speed Research Program. One of us (T.M.H.) has been supported for part of this period by a fellowship from the Foreign Ministry of France. We thank Alan Plumb for discussions and correspondences about this work.

## References

Anderson, J. G., and O. B. Toon, Airborne Arctic Stratospheric Expedition II: An overview, *Geophys. Res. Lett.*, *20*, 2499–2502, 1993.

Boering, K. A., B. C. Daube, S. C. Wofsey, M. Loewenstein, J. R. Podolske, and E. R. Keim, Tracer-tracer relationships and lower stratospheric dynamics: $CO_2$ and $N_2O$ correlations during SPADE, *Geophys. Res. Lett.*, *21*, 2567–2570, 1994.

Collins, J. E., G. W. Sachse, B. E. Anderson, A. J. Weinheimer, J. G. Walega, and B. A. Ridley, AASE-II in-situ tracer correlations of methane, nitrous oxide, and ozone as observed aboard the DC-8, *Geophys. Res. Lett.*, *20*, 2543–2546, 1993.

Conway, T. J., P. P. Tans, L. S. Waterman, K. W. Thoning, D. R. Kitzis, K. A. Masarie, and N. Zhang, Evidence for interannual variability of the carbon cycle from the National Oceanic and Atmospheric Administration/Climate Monitoring and Diagnostics Laboratory Global Air Sampling Network, *J. Geophys. Res.*, *99*, 22831–22855, 1994.

DeMore, W. B., D. M. Golden, R. F. Hampson, C. J. Howard, M. J. Kurylo, M. J. Molina, A. R. Ravishankara, and S. P. Sander, *JPL Publ. 87-41*, Jet Propul. Lab., Calif. Inst. of Technol., Pasadena, 1987.

Ehhalt, D. H., E. P. Röth, and U. Schmidt, On the temporal variance of stratospheric trace gas concentrations, *J. Atmos. Chem.*, *1*, 27–51, 1983.

Fahey, D. W., K. K. Kelly, S. R. Kawa, A. F. Tuck, M. Loewenstein, K. R. Chan, and L. E. Heidt, Observations of denitrification and dehydration in the winter polar stratospheres, *Nature*, *344*, 321–324, 1990.

Fung, I. Y., C. J. Tucker, and K. C. Prentice, Application of advanced very high resolution radiometer vegetation index to study atmosphere-biosphere exchange of $CO_2$, *J. Geophys. Res.*, *92*, 2999–3015, 1987.

Hall, T. M., and R. A. Plumb, Age as a diagnostic of stratospheric transport, *J. Geophys. Res.*, *99*, 1059–1070, 1994.

Hall, T. M., and M. J. Prather, Simulations of the trend and annual cycle in stratospheric $CO_2$, *J. Geophys. Res.*, *98*, 10,573–10,581, 1993.

Holton, J. R., Meridional distribution of stratospheric trace constituents, *J. Atmos. Sci.*, *43*, 1238–1242, 1986.

Houghton, J. T., B. A. Collander, and S. K. Varney, *Climate Change 1992: The Supplementary Report to the IPCC*

*Scientific Assessment*, Cambridge University Press, New York, 1992.

Jackman, C. H., R. K. Seals, and M. J. Prather, Two-dimensional intercomparisons of stratospheric models, *NASA Conf. Publ., 3042*, 1988.

Jones, R. L., and J. L. Pyle, Observations of $CH_4$ and $N_2O$ by the Nimbus-7 SAMS: A comparison with in situ data and two-dimensional numerical model calculations, *J. Geophys. Res., 89*, 5263–5279, 1984.

Keeling, C. D., R. B. Bacastow, A. F. Carter, S. C. Piper, T. P. Whorf, M. Heimann, W. G. Mook, and H. Roeloffzen, A three-dimensional model of atmospheric $CO_2$ transport based on observed winds, 1, Analysis of observational data, in *Aspects of Climate Variability in the Pacific and the Western Americas, Geophys. Monogr. Ser.*, vol. 55, edited by D. H. Peterson, pp. 165–236, AGU, Washington, D. C., 1989.

Ko, M. K. W., N. Sze, and D. K. Weisenstein, The roles of dynamical and chemical processes in determining the stratospheric concentration of ozone in one-dimensional and two-dimensional models, *J. Geophys. Res., 94*, 9889–9896, 1989.

Logan, J. A., M. J. Prather, S. C. Wofsy, and M. B. McElroy, Atmospheric chemistry: Response to human influence, *Philos. Trans. R. Soc. London A, 290*, 187–234, 1978.

Mahlman, J. D., H. Levy, and W. J. Moxim, Three-dimensional simulations of stratospheric $N_2O$: Predictions for other trace constituents, *J. Geophys. Res., 91*, 2687–2707, 1986.

McPeters, R., Ozone profile comparisons, in The Atmospheric Effects of Stratospheric Aircraft: Reports of the 1992 Models and Measurements Workshop, *NASA Ref. Publ., 1292*, D1–D37, 1993.

Murphy, M. M., D. M. Fahey, M. H. Proffitt, S. C. Liu, K. R. Chan, C. S. Eubank, S. R. Kawa, and K. K. Kelly, Reactive nitrogen and its correlation with ozone in the lower stratosphere and upper troposphere, *J. Geophys. Res., 98*, 8751–8773, 1993.

Pfister, L., and P. B. Russell, The tropical experiment of the Stratospheric-Tropospheric Exchange Project: Preface, *J. Geophys. Res., 98*, 8562, 1993.

Pfister, L., P. B. Russell, E. F. Danielson, and R. T. Watson, The Stratospheric-Tropospheric Exchange Project: Preface, *J. Geophys. Res., 96*, 17,400, 1991.

Plumb, R. A., and M. K. W. Ko, Interrelationships between mixing ratios of long-lived stratospheric constituents, *J. Geophys. Res., 97*, 10,145–10,156, 1992.

Podolske, J. R., M. Loewenstein, A. Weaver, S. E. Strahan, and K. R. Chan, Northern hemisphere nitrous oxide morphology during the 1989 AASE and the 1991-1992 AASE II campaigns, *Geophys. Res. Lett., 20*, 2535–2538, 1993.

Prather, M. J., Numerical advection by conservation of second-order moments, *J. Geophys. Res., 91*, 6671–6681, 1986.

Prather, M. J., M. M. García, R. Suozzo, and D. Rind, Global impact of the antarctic ozone hole: Dynamical dilution with a 3-D chemical transport model, *J. Geophys. Res., 95*, 3449–3471, 1990a.

Prather, M. J., M. B. McElroy, S. C. Wofsy, G. Russell, and D. Rind, Chemistry of the global troposphere: Fluorocarbons as tracers of air motion, *J. Geophys. Res., 92*, 6579–6613, 1987.

Prather, M. J., M. M. Garcia, A. R. Douglass, C. H. Jackman, M. K. W. Ko, and N. D. Sze, The space shuttle's impact on the stratosphere, *J. Geophys. Res., 95*, 18,583–18,590, 1990b.

Prather, M. J., and J. M. Rodriguez, Antarctic ozone: Meteoric control of $HNO_3$, *Geophys. Res. Lett., 15*, 1–4, 1988.

Proffitt, M. H., J. J. Margitan, K. K. Kelly, M. Loewenstein, J. R. Podolske, and K. R. Chan, Ozone loss in the Arctic polar vortex inferred from high-latitude aircraft measurements, *Nature, 347*, 31–36, 1990.

Remsberg, E., and W. Grose, Large-scale structures in $N_2O$ and $CH_4$, in The Atmospheric Effects of Stratospheric Aircraft: Reports of the 1992 Models and Measurements Workshop, *NASA Ref. Publ., 1292*, E1–E27, 1993.

Remsberg, E., and M. J. Prather, The Atmospheric Effects of Stratospheric Aircraft: Reports of the 1992 Models and Measurements Workshop, *NASA Ref. Publ., 1292*, 1993.

Rind, D., R. Suozzo, N. K. Balachandran, and M. J. Prather, Climate change and the middle atmosphere, 1, The doubled $CO_2$ climate, *J. Atmos. Sci., 47*, 475–494, 1990.

Schmidt, U., and A. Khedim, In situ measurements of carbon dioxide in the winter arctic vortex and at mid-latitudes: An indicator of the age of stratospheric air, *Geophys. Res. Lett., 18*, 763–766, 1991.

Schmidt, U., R. Bauer, A. Khedim, E. Klein, G. Kulessa, and C. Schiller, Profile observations of long-lived trace gases in the arctic vortex, *Geophys. Res. Lett., 18*, 767–770, 1991.

Schoeberl, M. R., M. H. Proffitt, K. K. Kelly, L. R. Lait, P. A. Newman, J. E. Rosenfield, M. Loewenstein, J. R. Podolske, S. E. Strahan, and K. R. Chan, Stratospheric constituent trends from ER-2 profile data, *Geophys. Res. Lett., 17*, 469–472, 1990.

Strahan, S. E., M. Loewenstein, J. R. Podolske, W. L. Starr, and K. R. Chan, Correlation of $N_2O$ and ozone in the southern polar vortex during the Airborne Antarctic Ozone Experiment, *J. Geophys. Res., 94*, 16,749–16,756, 1989.

Tuck, A. F., B. Watson, O. B. Toon, and S. Liu, The Airborne Antarctic Ozone Expedition: Preface, *J. Geophys. Res., 94*, 11,179, 1989.

Turco, R. P., A. Plumb, and E. Condon, The Airborne Arctic Stratospheric Expedition: Prologue, *Geophys. Res. Lett., 17*, 313–316, 1990.

---

T. M. Hall, CRC for Southern Hemisphere Meteorology, Monash University, 8 Redwood Drive, Notting Hill VIC 3168, Australia. (e-mail: hall@vortex.shm.monash.edu.au)

M. J. Prather, Earth System Science Department, University of California, Irvine, CA 92717. (e-mail: prather@halo.ps.uci.edu)

(Received July 5, 1994; revised December 5, 1994; accepted December 8, 1994.)